Am J Cancer Res 2024;14(1):274-299
www.ajcr.us /ISSN:2156-6976/ajcr0154147

Original Article

Altered gut microbiome drives heightened pain sensitivity in a murine model of metastatic triple-negative breast cancer

Rajib K Dutta[1], Yaa F Abu[1,2], Junyi Tao[1], Irina Chupikova[1], Janneth Oleas[1], Praveen K Singh[1], Nicolas A Vitari[1,2], Rehana Qureshi[3], Sundaram Ramakrishnan[1], Sabita Roy[1]

[1]Department of Surgery, University of Miami, Miami, FL 33136, USA; [2]Department of Microbiology and Immunology, University of Miami, Miami, FL 33136, USA; [3]Department of Pathology, University of Miami, Miami, FL 33136, USA

Received October 29, 2023; Accepted December 25, 2023; Epub January 15, 2024; Published January 30, 2024

Abstract: The microbiota residing in the gut environment is essential for host homeostasis. Increasing evidence suggests that microbial perturbation (dysbiosis) regulates cancer initiation and progression at local and distant sites. Here, we have identified microbial dysbiosis with the depletion of commensal bacteria as a host-intrinsic factor associated with metastatic dissemination to the bone. Using a mouse model of triple-negative mammary cancer, we demonstrate that a pre-established disruption of microbial homeostasis using an antibiotic cocktail increases tumor growth, enhanced circulating tumor cells, and subsequent dissemination to the bone. We found that the presence of pathogenic bacteria and loss of commensal bacteria in an antibiotic-induced gut environment is associated with sustained inflammation. Increased secretion of G-CSF and MMP-9 in intestinal tissues, followed by increased neutrophil infiltration and severe systemic inflammation in tumor-bearing mice, indicates the direct consequence of a dysbiotic microbiome. Increased neutrophil infiltration to the bone metastatic niche facilitates extravasation and transendothelial migration of tumor cells. It provides a novel, pre-established, and favorable environment to form an immunosuppressive pre-metastatic niche. The presence of tumor cells in immunosuppressive metastatic tumor niche disrupts the balance between osteoblasts and osteoclasts, promotes osteoclast differentiation, and remodels the bone structure. Excessive bone resorption by osteoclasts causes bone degradation and ultimately causes extreme pain in a bone metastatic mouse model. In clinical settings, bone metastasis is associated with intractable severe pain that severely compromises the quality of life in these patients.

Keywords: Breast cancer, pain, inflammation, microbial dysbiosis, bone metastasis

Introduction

Breast Cancer (BC) has been considered the second-highest cancer-related death in women after lung cancer, where one in 38 women (about 2.6%) will die from BC [1]. A recent American Cancer Society (ACS) report estimated 2.3 million new cases, leading to 685,000 deaths globally in 2020 [2]. Metastasis to the bone is the most common metastatic site in about 70% of all metastatic patients and the main reason for the high mortality rate among BC patients [3]. Bone metastasis is a debilitating condition commonly encountered in daily clinical practice, and patients with bone metastasis subsequently develop complications that need medical and surgical intervention. There is mounting evidence that chronic pain is a comorbidity associated with bone cancer metastasis that severely compromises the quality of life in these patients.

The gut microbiome has emerged as a key mediator of health and disease states. In a healthy state, gut microbiota and their metabolites regulate the innate and adaptive immune systems both locally and systemically [4]. On the other hand, disruption of the gut environment with the use of broad-spectrum antibiotics or chemotherapy alters the microbial community and leads to the development of chronic diseases like Cancer and inflammatory Bowel

https://doi.org/10.62347/LUJF9626

disease (IBD) [5, 6]. Growing evidence indicates the correlation between gut dysbiosis and breast cancer progression. A recent study by McKee et al. also shows that altering the gut microbiota aggravated breast tumor growth [7]. In the breast cancer model, tumor infiltration with *Fusobacterium nucleatum* promoted local tumor progression and metastases by suppressing T-cell accumulation in the tumor microenvironment [8]. Alternation of gut environment or dysbiosis of the gut microbiota and their metabolites is associated with sustained inflammation [9]. Of note, inflammatory cytokines and markers have been shown to be elevated in patients with metastatic breast cancer and are associated with a lower survival rate [10]. Gut dysbiosis can compromise gut barrier integrity and lead to bacterial translocation, ultimately developing a chronic inflammatory environment in the gut. It has been well established that chronic inflammation is associated with cancer growth and metastasis to distant organs. A recent study demonstrated that antibiotic-induced gut dysbiosis affects intestinal immune cells and thus alters their immune response, leading to accelerated bone metastasis [11].

Interestingly, microbial components from gut dysbiosis modulate neutrophil functions and regulate the inflammatory response. Moreover, Neutrophils are the prime component and regulator of the pre-metastatic niche in mouse breast cancer models. Neutrophil infiltration prepares the pre-metastatic sites before tumor cell migration and promotes metastasis without affecting the growth of primary tumors.

Once neutrophils infiltrate the bone metastatic niche, they facilitate the extravasation of tumor cells and provide a favorable environment to form metastasis [12]. Elevated neutrophil counts (Neutrophilia) and higher neutrophil-to-lymphocyte ratio are associated with tumor metastasis [13]. At the bone metastatic niche, neutrophils dampen the recruitment of other immune cells to the bone and suppress the resident anti-tumor immunity, causing an immunosuppressive microenvironment that promotes colonization and outgrowth of the disseminated tumor cells [14, 15]. Casbon et al. (2014) first reported that G-CSF could reconstruct the hematopoietic function of bone marrow and promote myeloid differentiation, thus increasing the number of neutrophils with immunosuppressive effect in breast cancer [16]. With this immunosuppressive environment, an influx of breast cancer cells hijack the normal bone remodeling process and induce bone resorption [17]. In bone metastatic niches, breast cancer cells release different factors that induce osteoclast differentiation, maturation, and activity [18]. The presence of cancer cells in the bone microenvironment disrupts the balance between osteoblasts and osteoclasts, leading to excess bone loss [19]. Also, studies have found that gut microbiota is involved in causing other bone diseases, like osteoarthritis and osteoporosis, through the brain-gut-bone axis. Increased osteoclast differentiation and osteolytic activity likely contribute to bone metastasis, creating space for tumor cells to infiltrate the bone microenvironment. However, very few studies have investigated the role of microbial dysbiosis in metastatic breast cancer.

The tumor microenvironment is complex, with metabolic interdependency between stromal, endothelial, and immune cells. Recent studies have revealed that neurons actively innervate the tumor microenvironment and promote tumor development and progression [20]. Tumor cells growing around existing nerves and the crosstalk between nerve cells and cancer cells, both systemically and locally, have emerged as a crucial hallmark of cancer progression. Studies have shown that cancer cells secrete several neurotrophic factors that induce nerve cells to invade and promote neurogenesis. On the other hand, neuronal cells secrete chemokines and neurotransmitters that essentially stimulate cancer cell proliferation, angiogenesis, and invasion. Thus, there is a reciprocal relationship between neurons and tumor cells.

Moreover, inflammatory cells such as proinflammatory macrophages and dendritic cells are recruited into the tumor microenvironment. Inflammation releases several pain-associated mediators and promotes neuronal plasticity and peripheral innervation. Inflammatory mediators such as NGF, endothelin's, VEGF, prostaglandins, bradykinin, and cytokines released by macrophages and other non-neuronal cells in tumor microenvironment can activate the

peripheral sensory fibers to induce inflammatory pain sensation [21].

Several recent studies have shown that antibiotic-induced gut microbiota disturbances drive metastatic dissemination in breast cancer patients and mammary cancer models [22, 23]. There is growing evidence that chronic pain is a co-morbidity associated with bone cancer metastasis. Very few studies have investigated the mechanism/s underlying antibiotic-induced gut dysbiosis that causes chronic pain in a bone metastatic pain model. In this study, we investigated how microbial dysbiosis associated with metastatic bone cancer contributes to chronic pain using clinically relevant orthotopic mouse BC models. We identified significantly increased primary tumor growth in animals treated with broad-spectrum antibiotics to disrupt gut microbiome. In antibiotic-treated mice, the presence of elevated pathogenic bacteria and loss of commensal bacterial species in the gut disrupt the gut homeostasis and induce inflammation. Increased neutrophil infiltration through the gut barrier allows tumor cells to infiltrate bone circulation. The presence of tumor cells creates a super-immunosuppressive metastatic tumor niche where tumor cells promote osteoclast differentiation and remodel the bone structure [24-26]. Excessive bone resorption by osteoclasts causes bone degradation and ultimately causes bone pain in a bone metastatic pain model.

Methods and materials

Animal

All animal experiments were performed in compliance with protocols approved by the Institutional Animal Care and Use Committee at the University of Miami, Miami, FL. 8-10 weeks female BALB/C mice were purchased from the Jackson Laboratory (Bar Harbor, ME) and used for the entire study. These mice were maintained at the University of Miami facility, with two to five mice housed in each cage kept in a 12-hour light-dark cycle with ad libitum access to food and water. Animals were randomly assigned for behavioral and biochemical analyses.

Cell culture

All cells were cultured at 37°C in a humidified atmosphere with 5% CO_2 in the air, and every two days, a fresh medium was added to the cells. Triple-negative breast cancer cell line (4T1-Luc) [American Type Culture Collection (ATCC)] were grown in high glucose DMEM (Thermofisher, Carlsbad, California, US) supplemented with 10% fetal bovine serum (FBS) (Hyclone, Thermofisher) and 100 units/mL penicillin/streptomycin (Pen/Strep) (Thermofisher). Cells were maintained at 37°C and 5% CO_2.

Mouse neuro-2a (N2a) neuroblastoma cells (ATCC® CCL-131™) were purchased from the American Type Culture Collection (Rockville, MD, USA). N2a cells were cultured in Dulbecco's modified Eagle medium (DMEM) supplemented with 10% (v/v) fetal bovine serum (FBS, Hyclone, Thermofisher) and containing 1% (v/v) antibiotics (100 U/mL penicillin, 100 mg/mL streptomycin) (Thermofisher). N2a cells were incubated at 37°C in a 5% CO_2 humidified atmosphere and passaged twice a week. N2a cells are broadly used to study the neuronal differentiation mechanism and neurite outgrowth.

Breast cancer model

For orthotopic xenograft assays, 50 µL of 5 × 10^5 4T1-Luc cells were suspended in 50 µL Matrigel and subcutaneously injected into the 4th mammary fat-pad of 10-12 weeks-old female BALB/C mice, using seven animals/group. Tumor growth was monitored by twice-weekly caliper measurement, and volumes were calculated as (long-side × short-side^2)/2. Primary tumors were removed when they reached 800 mm^3. Primary tumors were excised and stored for future experiences.

Behavioral tests

All behavioral experiments were carried out, with the investigators being blinded to treatment conditions. For von Frey testing, animals were habituated in boxes on an elevated metal mesh floor under stable room temperature and humidity for at least two days (30 minutes per day) before baseline testing. For Von Frey testing, mice were confined to individual 5 × 5 cm boxes placed on an elevated wire grid. A series of von Frey fibers with logarithmically increasing stiffness were applied to the plantar surface of the hind paw, and the paw withdrawal threshold (PWT) was calculated using the up-down method. A threshold force of response (in grams) was defined as the first filament that evoked at least two withdrawals out of five

applications. Seven or fewer filaments were applied to animals. Facial grooming is evaluated by counting the number of forepaws rubbing and hind paw scratching for 10 minutes. Heat sensitivity was tested using Hargreaves radiant heat apparatus (IITC Life Science). The hind paw withdrawal latency was recorded, with a cut-off of 20 seconds, to prevent tissue damage.

Cytokine and chemokines assays

After euthanasia, terminal blood was collected immediately through the cardiac puncture into endotoxin-free silicone-coated tubes without additives from control and tumor-bearing mice with/without antibiotics. The collected blood was allowed to clot at 25°C for 30 min, followed by centrifuging (1800 × g, 4°C, 15 min) to obtain serum. The serum specimens were preserved at -80°C. Cytokine and chemokine levels from mouse serum (1:1 dilution) were analyzed semi-quantitatively using the Luminex platform and done as a multiplex according to the manufacturer's instructions (R&D Systems) to assess circulating tumor-associated inflammatory mediator levels. Fluorescent-labeled beads coated with a specific capture antibody were added to each sample. After incubation and washing, a biotinylated detection antibody was added, followed by phycoerythrin-conjugated streptavidin. The beads were read on a Luminex instrument (Luminex 200 analyzer). Each cytokine level on the well was normalized to the intensity of the positive control sample. Signal intensity is graphed in arbitrary units versus control expressed as one.

RNA isolation from 4T1-Luc and neuro-2a cells and first-strand cDNA synthesis

ACCORDING TO THE MANUFACTURER'S INSTRUCTIONS, total RNA from 4T1-Luc and Neuro-2a cells were isolated using an RNeasy Mini Kit (Qiagen, Gaithersburg, MD, USA, Cat# 74104). First, DNase I, RNase-free (Westlake, LA, USA, Cat# M0303S) treatment, was used to digest contaminated genomic DNA. Then, to check the integrity and overall quality of isolated RNAs, two μg RNAs were applied to Agilent 2100 Bioanalyzer to measure RNA quality by determination of absorbance at 260 and 280. Next, the cDNA was synthesized using the RT2 First Strand Kit (Qiagen, Valencia, CA, USA) following the manufacturer's instructions.

Real-time RT^2 profiler PCR array

Eighty-four genes or biological pathways involved in mediating communication between tumor cells and the cellular mediators of inflammation and immunity were analyzed using the RT2 Profiler Cancer Inflammation and Immunity Crosstalk PCR Array (Qiagen, Gaithersburg, MD, USA). According to the manufacturer's protocol, the high-quality cDNAs were used on the real-time RT^2 Profiler PCR Array in combination with Applied Biosystems SYBR™ Green PCR Master Mix (Cat. no. 4312704). A 102-μL cDNA synthesis reaction volume was mixed with 2 × RT2 SYBR Green Master mix and RNase-free water to obtain a total volume of 2,700 μL. Subsequently, 25 μL of the PCR component mix was placed into each well of the PCR array (a 96-well array). The three steps of the cycling program were 95°C for 10 min for one cycle, followed by 40 cycles of 95°C for 15 s and 60°C for 60 s. This process was repeated for 40 cycles using the ABI-7500 (Applied Biosystems, Waltham, MA, USA). The expression levels were quantified relative to the values obtained for housekeeping genes (ACTB, B2M, GAPDH, HPRT1, and RPLP0). The PCR array was performed in triplicate.

Analysis of real-time RT^2 profiler PCR array

Online Analysis Software (https://geneglobe.qiagen.com/us/analyze) was used to analyze PCR Array data. All plates had three positive PCR controls and three reverse-transcription controls. Calculations of contamination with mouse genomic DNA, according to the manufacturer's instructions, showed the presence of genomic DNA in an acceptable range that would not influence experiment performance. The cycle threshold (Ct) values obtained in quantification were used to calculate fold changes in mRNA abundance. The average was chosen from the group of six housekeeping genes as the varying reference genes. Changes in mRNA level for evaluated genes were assessed in all groups in relation to the control group of animals, with mRNA abundance set up arbitrarily as 1.

In vivo bioluminescence imaging

Before in vivo imaging, mice were shaved in the region of interest depicted in the figure. Then, bioluminescence images of 4T1-Luc2 cells

bearing mice were captured using the IVIS Spectrum CT Pre-Clinical In Vivo Imaging System (PerkinElmer, MA, USA) 15 min after intraperitoneal injection with 10 µL/g of body weight with a solution of Luciferin (PerkinElmer) prepared in PBS at 15 mg/mL. Imaging was performed on days 7, 10, 17, and 22 for the orthotopic injection model. Total photon flux (photons per second) was analyzed from a fixed region of interest (ROI) in the tumor area using Living Image 4.50 software from PerkinElmer. A control (noninjected) mouse was used for analysis, and the average radiance of each tissue was subtracted from the average radiance of the injected mice.

Bone marrow collection

After euthanization, tibia and femur bones were carefully removed and kept in a Petri dish placed on ice. The muscles surrounding the femur were gently removed, followed by gentle separation of the distal epiphysis from the femoral shaft using a tweezer. Then, the ends of the tibia and femur bones were cut by a scalpel blade to expose the marrow, followed by inserting a 25-gauge needle into the distal end of the femur and injection of 1 ml cold complete media (Gibco, Thermo Fisher Scientific) and collected in a 15-ml tube. We then inverted the bone to flush twice from the proximal end, and cells were centrifuged at 800 × g for 5 min at 4°C. Cells pellet were washed with cold PBS/EDTA buffer followed by filtering through a 70-µm mesh cell strainer for subsequent detections.

Flow cytometry

To analyze the immune subsets, present within the bone marrow tumor microenvironment, cells from bone were harvested (described previously) and treated with 1 × RBC lysis buffer (Sigma) to reduce red blood cell contamination. They were counted with 2×10^6 cells per sample and fixed by 4% paraformaldehyde (PFA). The cells were blocked and permeabilized by Fc receptor staining buffer containing 1 µg/ml of anti-mouse-CD16/CD32 (101302, Biolegend), 2.4 G2, 2% FBS, 5% NRS, 2% NMS, 0.1% Triton X-100 in HBSS (BD bioscience) for 30 min at room temperature. Cells were washed with PBS and pelleted, followed by each sample being transferred to a well of a U-bottomed 96 well plate before proceeding with antibody staining. An antibody master mix containing all antibodies used for staining was prepared in PBS to a total volume of 100 µl per sample. Cells were washed after staining with staining buffer and fixed with fixation buffer (BioLegend). Samples were washed once with PBS with EDTA, and finally, flow cytometry events were acquired using a Cytek Aurora flow cytometer. Data were analyzed using SpectroFlo software (version 10.8.0; Tree Star, Ashland, OR).

Fecal sample collection and DNA extraction

Fecal samples from the distal colon region were collected in 1.5 ml RNase/DNase-free tubes (ThermoFisher Scientific) at various time points. The fecal samples were immediately frozen on dry ice and then stored at -80°C. Samples were lysed using glass beads in MagnaLyser tissue disruptor (Roche, Indianapolis, IA), and total DNA was isolated using Power-soil/Fecal DNA Isolation Kit (Mo-Bio, Carlsbad, CA) as per the manufacturer's specifications. All extracted DNA samples were stored at -80°C until amplification.

16S rRNA gene sequencing

The University of Minnesota Genomics Center performed sequencing. The hypervariable V4 region of the 16S rRNA gene was PCR amplified using the forward primer 515F (GTGCCAFCMGCCGCGGTAA), reverse primer 806R (GGACTACHVGGGTWTCTAAT), Illumina adaptors, and molecular barcodes to produce 427-bp amplicons. Amplicons were sequenced with the Illumina MiSeq version 3 platform, generating 300-bp paired-end reads. Unfortunately, the extraction controls could not be PCR amplified due to the very low copy number (less than 10 in extraction control versus 10e-8 copies in experimental samples) and were therefore excluded from the sequencing process.

Bioinformatics analysis

Demultiplexed sequence reads were clustered into amplicon sequence variants (ASVs) with the DADA2 package (version 1.21.0) [27] implemented in R (version 4.0.3) and RStudio (version 1.1.463). The steps of the DADA2 pipeline include error filtering, trimming, learning of error rates, denoising, merging of paired reads, and removal of chimeras. On average, 26,800

sequence reads per large intestine sample (Table S1) were kept after error filtering and other steps. The ASV table generated by DADA2 was imported into the QIIME2 pipeline [28] for diversity analyses and taxonomic assignment. Diversity analyses were performed by using the qiime diversity core-metrics-phylogenetic script with a sampling depth of 15,000 for large intestine samples. Taxonomic assignment of ASVs was performed to the genus level using a naive Bayesian classifier [29] implemented in QIIME2 with the Greengenes reference database (13_8 99%) [30]. MicrobiomeAnalyst [31] was used for generating scatter bar plots and LefSe (Linear discriminant analysis Effect Size) [32] plots. The threshold on the logarithmic LDA score for discriminative features was set to 2. The cut-off for false discovery rate-adjusted *p*-value (q-value) was set to 0.1 for LEfSe analysis. PICRUSt [33] was implemented within the galaxy app (https://huttenhower.sph.harvard.edu/galaxy/) to predict the functional composition of a metagenome using 16S data with reference genomes from Greengenes [30] and IMG [34] databases. KEGG orthologs [35] were used to predict metagenome. KEGG pathway was categorized to pathway hierarchy level 2. STAMP [36] was used to identify differentially abundant pathways and generate extended error bar plots. BugBase [37] phenotype predictions were implemented using the online web app (https://bugbase.cs.umn.edu/) to predict high-level phenotypes present in microbiome samples using 16S amplicon data.

Statistical analysis

GraphPad Prism 8 (GraphPad Software, Inc.) was used for experimental data analysis and plotting. Parametric data were compared using Student's t-test. Quantitative data are expressed as means ± SEM of three experiments. The Kruskal-Walli's test was used to detect if α diversity differed across treatments. Permutational multivariate analysis of variance (PERMANOVA) was used to detect if β diversity differed across treatments. Benjamini-Hochberg method was used to control the false discovery rate (q-value). The student's t-test was used to analyze the data differences between the two groups. One-way ANOVA followed by Tukey's or Dunnett's multiple comparison tests was used to analyze the data with more than two groups. To ensure reproducibility, all experiments were repeated at least three times. All results were considered statistically significant if $P < 0.05$.

Results

Development of breast cancer bone metastatic model and assessment of mechanical and thermal hyperalgesia in mice

A triple negative mouse mammary cancer cell line, 4T1, transfected with Luciferase, was used to establish a metastatic breast cancer model. 4T1-Luc cells were injected orthotopically in the fourth mammary gland of 12-week-old female BALB/c mice as described [38] (**Figure 1A**). Orthotopic injection leads to spontaneous metastasis of the lungs, lymph nodes, liver, brain, and bone [39]. As expected, significantly increased expression of 4T1-Luc breast cancer cells was detected in the bone marrow, indicating bone metastasis (Figure S1A). Bone metastasis was also investigated by staining the cytokeratin-positive cells in the bone marrow, and the result demonstrated that cytokeratin-positive cells in the marrow are indeed tumor cells, further validating our model (Figure S1B). Since about 50-70% of metastatic breast cancer patients develop liver metastases, and 5% to 12% of these patients develop liver metastases during cancer recurrence [40, 41]. We investigated the liver and lungs for metastases. Tumor-bearing mice showed increased liver weight to control, and metastatic nodules were visible in the gross morphology of the liver and lungs (Figure S1C and S1D).

In parallel, we evaluated pain sensitivity in mice with metastatic breast cancer to bone compared with control mice (**Figure 1B**). Our results indicated increased mechanical and thermal pain sensitivity in mice by von Fray, tail flick, and hot plate methods during tumor growth. Compared to controls, mice with metastatic breast cancer were found to have decreased latency to Von Frey, Hot Plate, and Tail Flick response (**Figure 1C-E**), which collectively indicate heightened pain sensitivity. Remarkably, these results persisted 38 days post-tumor injection, indicating long-term hypersensitivity to thermal and mechanical pain sensitivity in the murine model of metastatic breast cancer to bone.

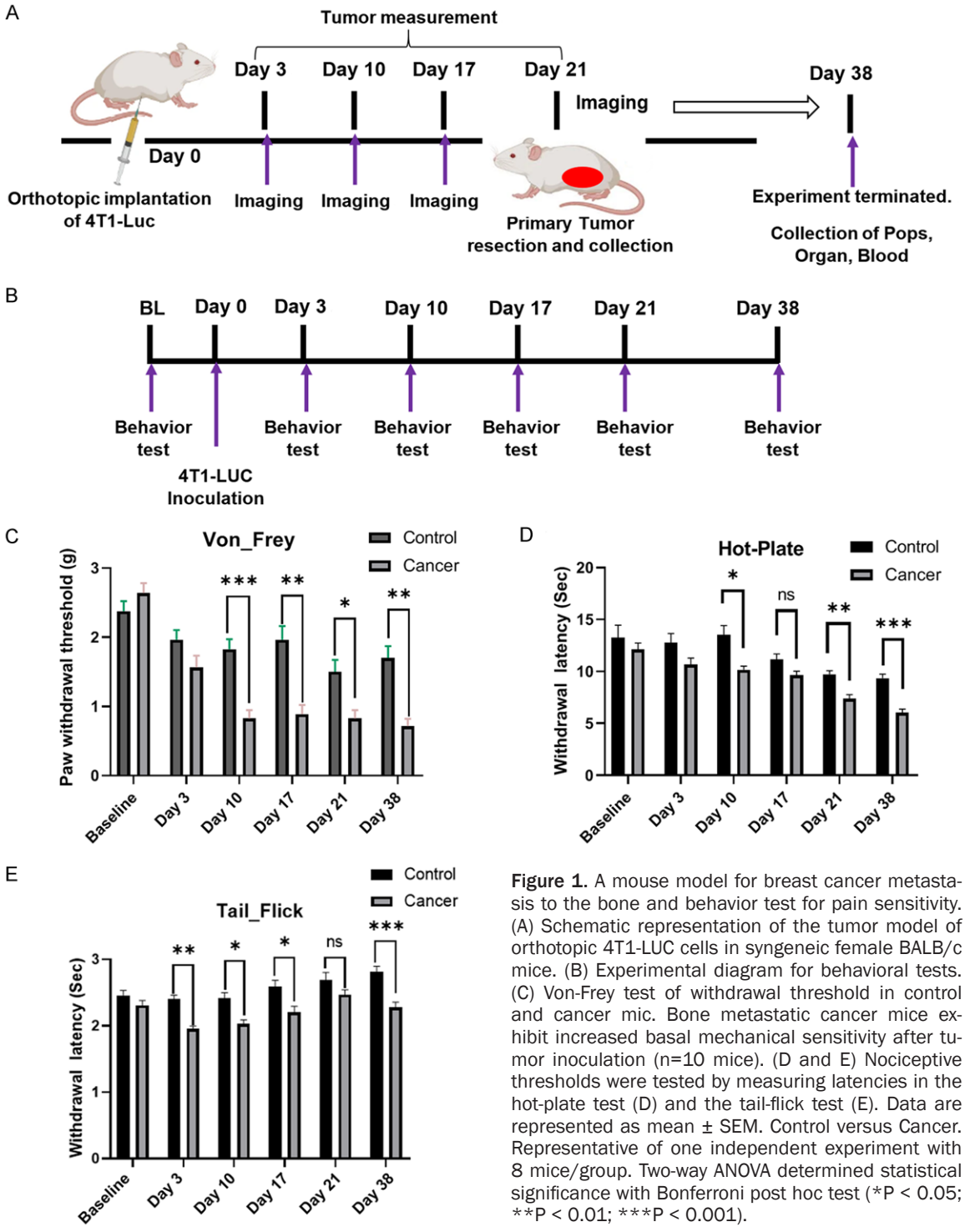

Figure 1. A mouse model for breast cancer metastasis to the bone and behavior test for pain sensitivity. (A) Schematic representation of the tumor model of orthotopic 4T1-LUC cells in syngeneic female BALB/c mice. (B) Experimental diagram for behavioral tests. (C) Von-Frey test of withdrawal threshold in control and cancer mic. Bone metastatic cancer mice exhibit increased basal mechanical sensitivity after tumor inoculation (n=10 mice). (D and E) Nociceptive thresholds were tested by measuring latencies in the hot-plate test (D) and the tail-flick test (E). Data are represented as mean ± SEM. Control versus Cancer. Representative of one independent experiment with 8 mice/group. Two-way ANOVA determined statistical significance with Bonferroni post hoc test (*P < 0.05; **P < 0.01; ***P < 0.001).

Gut microbiota mediate increased pain sensitivity in murine models of metastatic breast cancer to bone

Previous studies have revealed the profound role of gut microbiota in modulating pain sensitivity [42, 43]. To evaluate whether pain in our murine model of breast cancer metastasis to bone is associated with microbial dysbiosis, 16S rRNA sequencing was performed on intestinal contents collected from control or bone metastatic breast cancer (BMBC) mice on the day of sacrifice, which is 38 days post cancer implantation. On average, we obtained 26,800

sequence reads per stool sample and identified 542 unique ASVs (Table S2). The two "non-phylogeny-based" metrics, the Shannon index and Chao1, were used to measure α-diversity. In the intestine, the Shannon index, which accounts for both abundance and evenness, showed significant differences between the control and cancer groups ($P < 0.005$), as the cancer group mice exhibited a significant increase in alpha diversity compared with the control group (**Figure 2A**). The Chao1 diversity analysis also indicated a significant increase in operational taxonomic unit (OTU) richness in the cancer group ($P < 0.01$) (**Figure 2A**). Moreover, β diversity was assessed by Bray-Curtis revealed that the cancer group has significantly distinct clustering of bacterial communities compared to control mice ($P < 0.01$) (**Figure 2B**). Further analysis by LefSe (Linear Discriminant Analysis (LDA) Effect Size) analysis was performed to determine the bacterial taxa that were differentially enriched and revealed that a net expansion of the relative abundance of Bacteroidota, Actinobacteriota, Proteobacteria and a reduction of Firmicutes in the intestine of the cancer group compared to control mice (**Figure 2C**). A group-wise comparison revealed that the decreased abundance of the Lactobacillaceae family and increased abundance of Micrococcaceae, Mitochondria family observed on BMBC mice after cancer cells implantation (**Figure 2D**).

Stack bar graphs show the relative abundance of several bacterial taxa at the phylum level per two treatment groups (Figure S2A). A group-wise comparison revealed that the decreased abundance of the phylum Firmicutes and increased abundance of the Proteobacteria, Bacteroidota, and Actinobacteriota were observed after cancer cell implantation (Figure S2B).

Further analysis of taxonomic groups between BMBC and control mice revealed the enrichment of pathogenic bacteria at the genus level in the cancer group, as represented by Staphylococcus, Rothia, and Lachnospiraceae (Figure S2C). Additionally, Lactobacillus, known to prevent inflammation and maintain barrier function, was significantly reduced in the BMBC mice.

Overall, our results show that cancer growth significantly altered the large intestine microbiome. These results suggest a strong correlation between gut dysbiosis and subsequent increased sensitivity to pain in cancer-bearing mice.

A sustained proinflammatory state is associated with microbial dysbiosis

Inflammatory cytokines have been shown to be elevated in patients with metastatic breast cancer and are associated with a lower survival rate [44, 45]. Microbial dysbiosis is associated with sustained inflammation and contributes to pain due to persistent proinflammatory immune cell activation [46, 47]. Immune cell activation is associated with hyperactivity of the transcription factor NF-κB and overexpression of inflammatory cytokines [48]. Also, in intestinal tissue, chemokine and cytokine secretion by immune as well as intestinal epithelial cells (IECs) can cause inflammation of the tissues and regulate immune cell homeostasis. In order to investigate the effect of gut microbial dysbiosis on intestinal immune homeostasis, inflammatory markers were profiled from serum samples of bone metastatic breast cancer models. We found that the Granulocyte-colony-stimulating factor (G-CSF) and Matrix metalloproteinase-9 (MMP-9) levels are significantly higher in the systemic circulation of metastatic breast cancer mice than in the control mice (**Figure 3A** and **3B**). Under physiological conditions, the G-CSF concentration in plasma is almost undetectable. However, in breast cancer patients' plasma, granulocyte colony-stimulating factor (G-CSF) is significantly higher than healthy controls [49]. The mucosal environment's innate and adaptive immune system interacts with gut commensal bacteria; intestinal homeostasis is maintained by exhibiting tolerance toward commensals and proinflammatory responses toward pathogens [50].

Moreover, intestinal microbial dysbiosis has been shown to activate the immune system and promote a proinflammatory environment at the intestinal mucosal surface [42]. 16S rRNA sequencing results revealed a significant decrease in Firmicutes/Bacteroidetes ratio in bone metastatic breast cancer mice compared to the control group. An overgrowth of the pathogenic phylum Bacteroidetes and a substantial depletion of the commensal genus Lactobacillus in the intestinal lumen of mor-

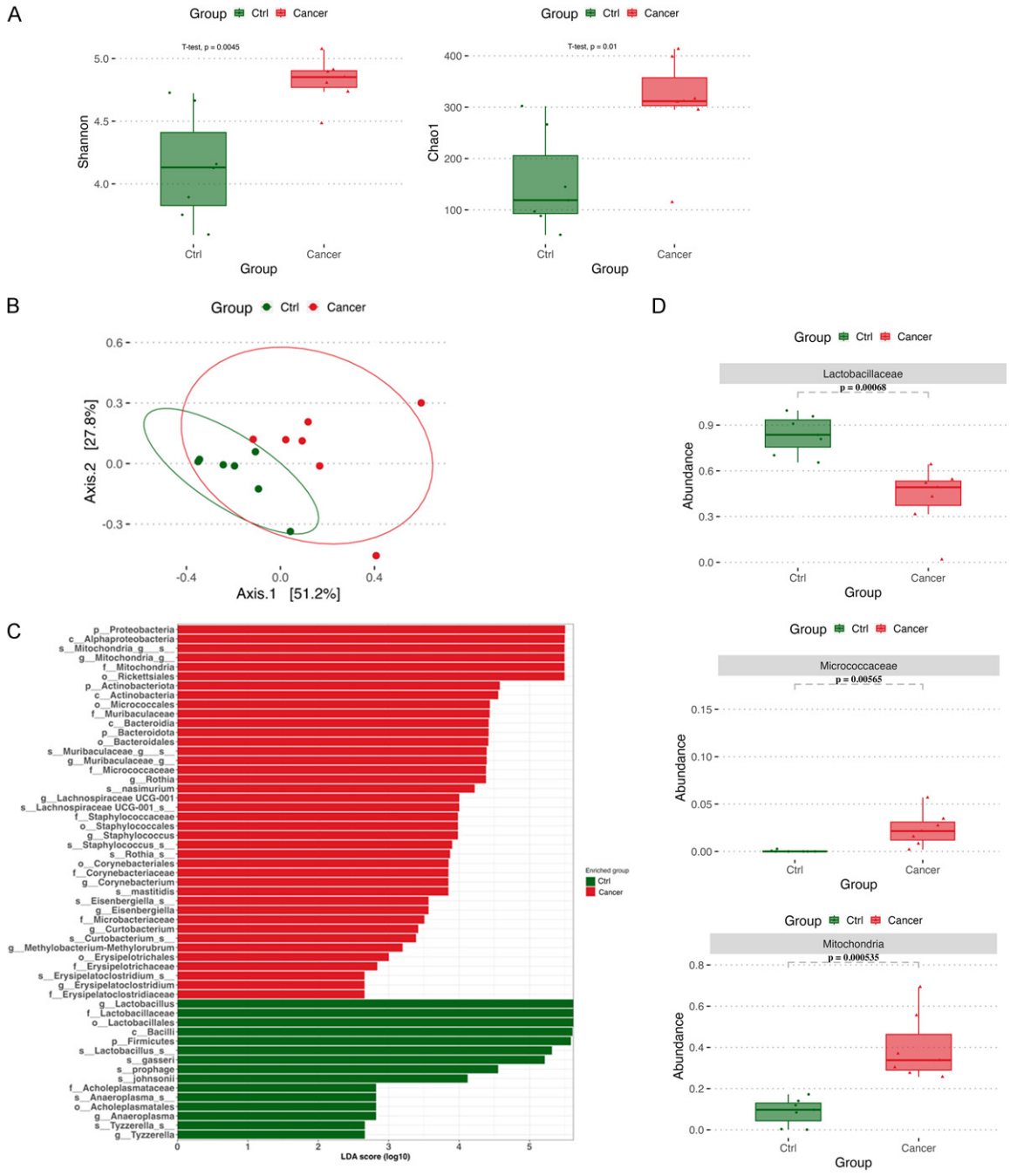

Figure 2. Cancer implantation induces gut microbial dysbiosis in cancer mice. A. The Shannon and Chao1 index show α-diversity. A t-test was conducted on the Shannon and Chao1 index. Alpha diversity analysis using Shannon and Chao1 index shows increased alpha diversity in the cancer mice group compared to the control group. B. β-diversity significantly differed between the Cancer and control groups using Bray-Curtis. C. Lefsa plots show changes in the abundance of bacteria at phylum, family, and genus levels. D. Tukey's box plots show the relative abundance of the bacterial family significantly changing among cancer and control mice-data represented as bar plots with SEM. Data were analyzed by one-way ANOVA with post-hoc Tukey's test.

phine-treated mice highlighted intestinal inflammation is associated with increased monocyte infiltration in the intestinal lumen [51]. Increased infiltration of monocyte-secreted G-CSF causes systemic and local intestinal tissue inflammation. In addition, increased

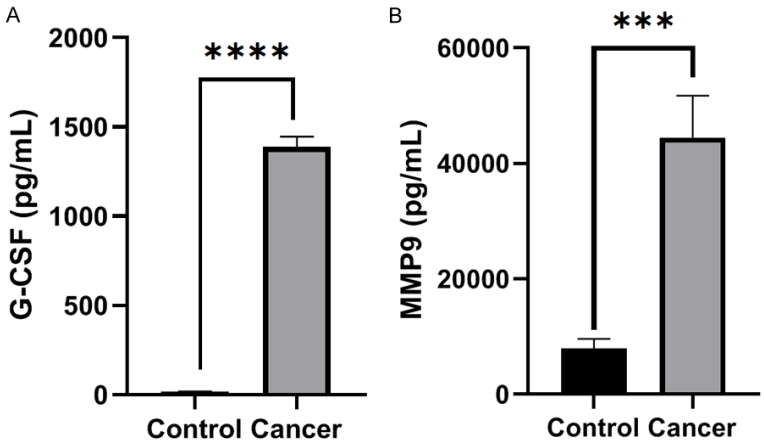

Figure 3. Inflammatory markers expression. The serum was collected from control and Bone metastatic breast cancer mice. G-CSF and MMP9 levels were measured and analyzed using Luminex multiplex assay. A. Serum levels of G-CSF. B. Serum levels of CXCL1. n=10/group from one experiment was performed, and data was represented as bar plots with SEM. *P < 0.05, **P < 0.01, and ***P < 0.001 versus naive controls (Data were analyzed by student's t-test).

expression of G-CSF is associated with neutrophil recruitment. G-CSF is known to be produced locally in inflamed tissues and released into the circulation, leading to neutrophil mobilization from the bone marrow or even affecting their numbers in the bone marrow. On the other hand, MMP9 is undetectable in healthy tissue, although highly upregulated during inflammation and cancer [52]. Increased expression of MMP-9 by circulatory neutrophils plays a role in basement membrane degradation, promoting migration, invasion, and metastases to the bone [53].

To investigate the role of increased circulation of neutrophils in creating bone metastatic niches, we utilized flow cytometry to profile the primary immune cell populations within the bone marrow (BM) of normal mice compared to BM at end-stage from mice injected with 4T1-Luc cells. Mounting evidence had shown that at this time point, most of the 4T1-Luc injected orthotopic mice have bone metastases. Compared to controls, analysis of immune cell populations revealed a significant decrease in leukocytes (**Figure 4A**) in 4T1-Luc injected mice. The population of neutrophils identified by the Ly6G surface marker was found to be significantly high in cancer-bearing mice (**Figure 4B**). Along with the neutrophil population, the macrophage cell population defined by F4/80 was also found to be significantly higher in 4T1-Luc injected cancer mice (**Figure 4D**). However, we did find a decreased number of monocytic cells in the bone marrow cell population, which could be due to rapid differentiation into macrophages, which was observed to be elevated (**Figure 4C**). Moreover, we found a decrease in NK cells and B-cells characterized by $CD49^+$ and $CD19^+$ respectively (**Figure 4E** and **4I**). Analysis of lymphocytic cells revealed a decrease in the populations of T lymphocytes (**Figure 4F**). Specifically, CD4+ and CD8+ T cells were decreased in the BM of 4T1-Luc injected mice (**Figure 4G** and **4H**). These findings suggest that the formation of bone metastases may be associated with immune suppression in the BM.

The spleen is a major site of extramedullary hematopoiesis and was shown to be the origin of MDSCs in cancer. Interestingly, we observed significant splenomegaly in mice injected in the 4T1-Luc implanted BMBC group, suggesting that immune modulation during the formation of bone metastases is systemic. Moreover, the increase in BM granulocytes and decrease in T cells correlated with the increase in spleen weight, supporting the hypothesis that the enhanced granulocyte population may be immunosuppressive. Taken together, these results imply that the formation of bone metastasis is associated not only with the accumulation of granulocytes and decreased T cells but also with the acquisition of an immunosuppressive phenotype. Along with immunosuppressive function, myeloid-derived suppressor cells, including neutrophils and macrophages, have the potential to differentiate into osteoclasts, which might subsequently promote bone loss in bone metastasis and cause severe pain in bone metastatic breast cancer mouse model [54, 55].

Antibiotic treatment accelerates tumor growth in metastatic breast cancer and induces severe pain

Breast cancer patients who use antibiotics within three years of diagnosis have an increased risk of death. A recent large study conducted by Australian researchers on more

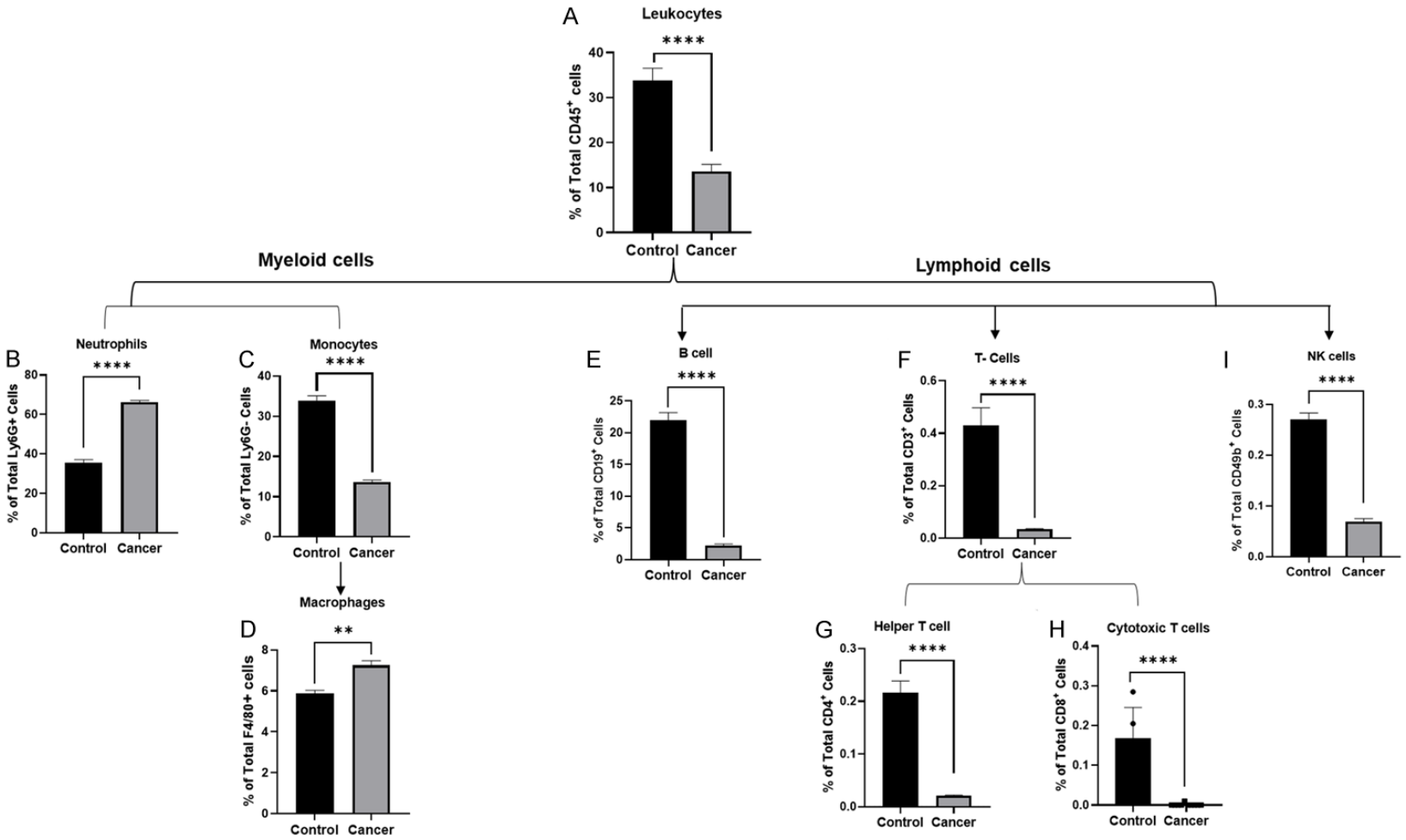

Figure 4. Immunosuppressive environment of bone marrow in bone metastatic breast cancer (BMBC) mouse model. (A-I) Bar plots showing mean (SEM) percentages of total leukocytes (A), myeloid cells including Neutrophils (B), Monocytes (C), Macrophages (D), lymphoid cells including B-cells (E), T-cells (F), TH-cells (G), TC-cells (H), and NK-cells (I) tumor-infiltrating populations as determined by flow cytometry. Data represented as bar plots with SEM. Data were analyzed by one-way ANOVA with post-hoc Tukey's test. *P < 0.05, ***P < 0.001, ****P < 0.0001.

than 7000 patients with breast cancer patients found an association between antibiotic use in the six months prior to the patient's diagnosis and poorer survival [56]. A recent study demonstrated that exposure to antibiotics may cause gut microbiome dysbiosis that causes a decrease in the number of immune cells in circulation and correlates with poor outcomes [22]. Using mouse models of breast cancer, another study has also suggested an association between antibiotic-induced gut microbiome dysbiosis and increased tumor growth [7]. To further investigate if gut microbial dysbiosis contributed to antibiotic-induced breast cancer progression and hypersensitivity, we used orthotopic mammary fat pad injection mouse model with 4T1-Luc cell line (**Figure 1A**). Prior to the orthotopic injection, BALB/c female mice were administered a cocktail of antibiotics consisting of vancomycin, neomycin, metronidazole, amphotericin, and ampicillin for 10 days. Antibiotic treatment was continued throughout the experimental period, following the regimen illustrated in **Figure 5A** to maintain a continuous removal of the microbiota from the gut environment. Microbiome data showed that treating mice with antibiotics markedly reduced gut bacterial content but not completely depleted, which persisted throughout the experimental time course. Strikingly, mice treated with antibiotic cocktails have been found to have accelerated tumor growth compared to control mice (**Figure 5B**).

Behavior tests of cancer pain for assessing mechanical sensitivity by von Frey test were performed on days 10, 0, 7, 12, 18, 23, and 42 after 4T1-Luc cells inoculation (**Figure 5C**). On day 10 before antibiotic cocktail treatment, the baseline pain sensitivity of female BALB/c mice was measured, and mice were assigned in groups in a way that each group had equal baseline pain sensitivity. On day 0 before tumor cells, inoculation, Antibiotic (Abx) treatment groups Abx and Cancer+Antibiotics (Can+Abx) showed an increase in paw-withdrawal frequency in von Frey tests compared to the other two groups (control and cancer, although cancer cells were not implanted yet). This data shows antibiotics cause increased pain sensitivity in mice. On day 7, after tumor inoculation, the Abx-treated, tumor-bearing mice group only developed mechanical allodynia in the hind paws. This sign of cancer pain was significantly maintained on days 12, 18, and 23 in both cancer and Can+Abx mice. Tumors were surgically removed from mice on day 23 due to their increased growth rate. On day 38, after 4T1-Luc cells inoculation (15 days after tumor removal), cancer and antibiotic-treated cancer groups exhibited persistent pain sensitivity. Although the pain sensitivity between the cancer group and the antibiotic-treated cancer group is not significantly different, the results clearly showed that antibiotic-treated tumor-bearing mice exhibited more pain than only cancer group mice without antibiotics. Increased tumor volume and excessive pain sensitivity in antibiotic-treated tumor-bearing mice indicate that dissemination of cancer cells to the bone is likely to increase following disruption of gut homeostasis; the progression of metastatic burden is accelerated in antibiotic-treated animals, similarly to primary tumor growth. Thus, we focused on exploring what drives the enhanced primary tumor growth and increased pain accompanying a perturbed microbiota.

The use of broad-spectrum antibiotic predominantly disrupts the gut ecosystem and increase the number of pathogenic bacteria

Next, we focused on exploring the role of gut microbiome dysbiosis in driving enhanced primary tumor growth in antibiotic-treated cancer mice. Fecal samples were collected on the day of mice sacrifice from the Control, Cancer, Antibiotics (Abx), and Cancer+Antibiotics (Can+Abx) groups and were subjected to 16S rRNA sequencing. On average, we obtained 26,800 sequence reads per stool sample and identified 542 unique ASVs (Tables S1, S2). Overall, our results showed that cancer growth had changed the large intestine microbiome while the Abx treatment continued to have a long-lasting effect on the large intestinal microbiome. β diversity was assessed by Bray-Curtis distances and visualized with PCoA plots. Analysis of β diversity showed that the Cancer group was significantly different from the control ($P < 0.05$) (**Figure 6A**). Moreover, the Can+Abx group was substantially different from cancer or control ($P < 0.05$) (**Figure 6A**).

Shannon's diversity index measured the α-diversity. At a sequencing depth of 15,000, Shannon's diversity index was significantly lower in the Can+Abx group than in either the

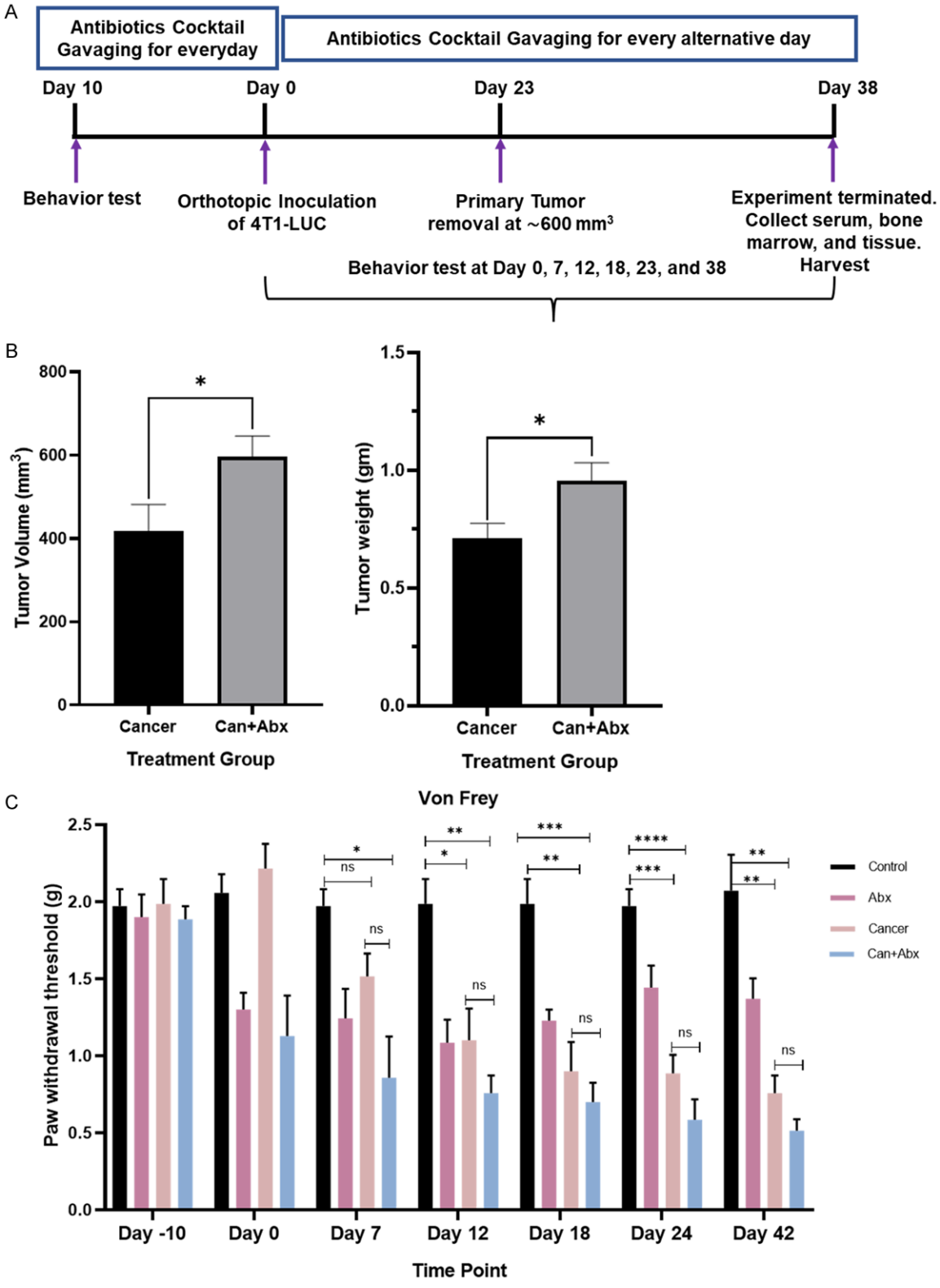

Figure 5. Antibiotic-induced gut microbial dysbiosis accelerates bone metastasis breast cancer in a mouse model. A. Schematic of the experimental timeline: antibiotics were administered orally every day for the first 10 days until orthotopic injection; after that, mice were gavaged every alternative day for the duration of the experiment until cessation 38 days after orthotopic injection. B. Changes in tumor weight and volume were evaluated on day 23 after orthotopic cell injection in each group. The data are presented as the mean ± SEM. n=7-10 mice in each group. *P < 0.05, difference relative to the cancer group. C. Von Frey testing to determine antibiotic-induced mechanical allodynia, as assessed by withdrawal threshold in mice treated with vehicle or cancer mice. n=7-10 mice. Data displayed represent the mean ± SEM, two-tailed Student's t-test, *P ≤ 0.05; **P ≤ 0.01; ***P ≤ 0.001.

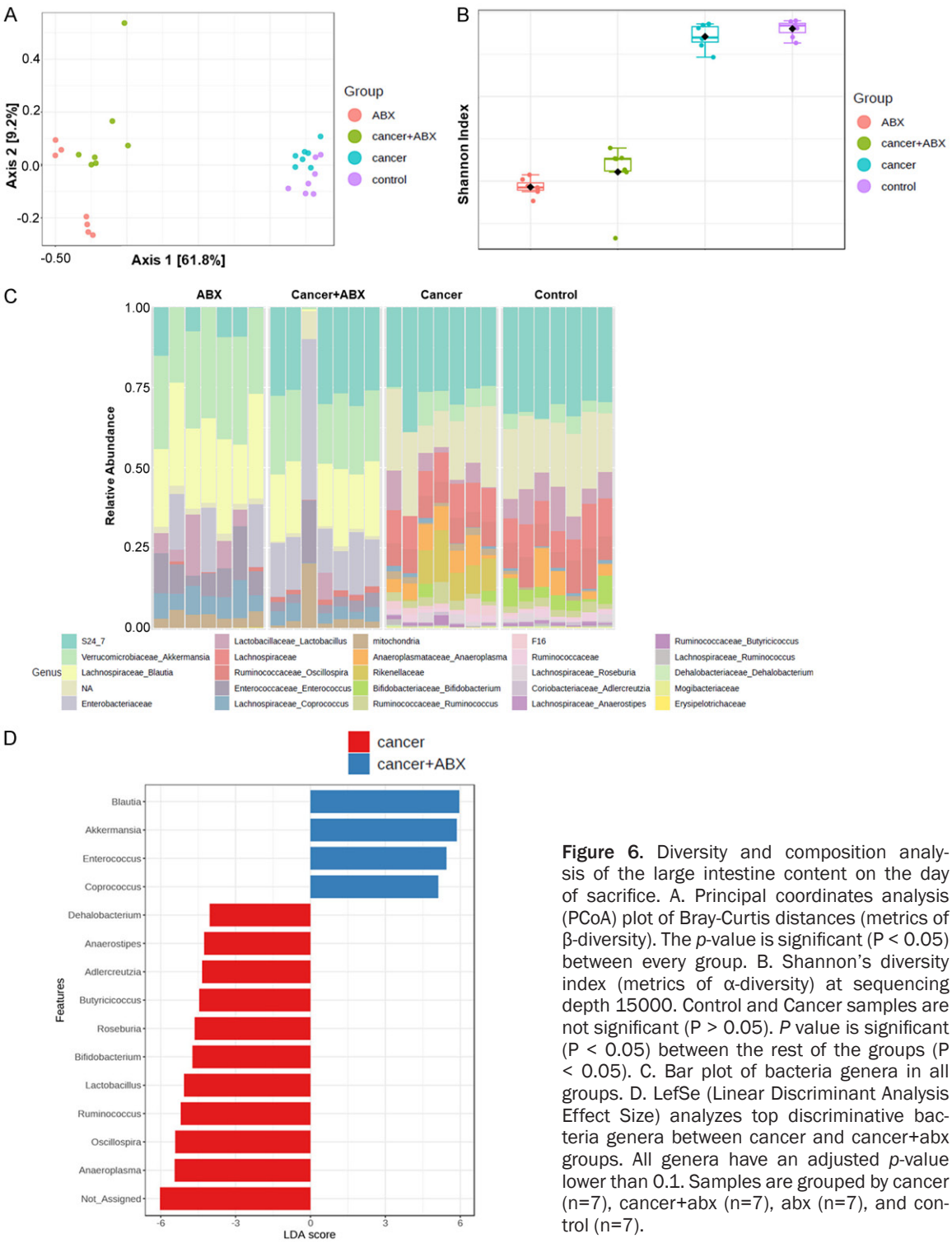

Figure 6. Diversity and composition analysis of the large intestine content on the day of sacrifice. A. Principal coordinates analysis (PCoA) plot of Bray-Curtis distances (metrics of β-diversity). The *p*-value is significant ($P < 0.05$) between every group. B. Shannon's diversity index (metrics of α-diversity) at sequencing depth 15000. Control and Cancer samples are not significant ($P > 0.05$). *P* value is significant ($P < 0.05$) between the rest of the groups ($P < 0.05$). C. Bar plot of bacteria genera in all groups. D. LefSe (Linear Discriminant Analysis Effect Size) analyzes top discriminative bacteria genera between cancer and cancer+abx groups. All genera have an adjusted *p*-value lower than 0.1. Samples are grouped by cancer (n=7), cancer+abx (n=7), abx (n=7), and control (n=7).

cancer or control group ($P < 0.01$) (**Figure 6B**), which was consistent with the expected effect of Abx. There was no difference between the control and cancer group ($P > 0.05$) (**Figure 6B**). The diversity result indicated the Abx was having a long-term effect on the intestinal microbiome, and the effect was independent of the cancer effect.

The bar plot of bacteria was plotted at the genus level (**Figure 6C**). Visually, the Abx groups (Abx and Can+Abx) were very different from non-Abx groups (control and cancer). LefSe (Linear Discriminant Analysis (LDA) Effect Size) analysis was performed between Cancer and Can+Abx groups to determine the bacterial taxa that were differentially enriched (**Figure 6D**). The analysis was performed at the genus level. At the genus level, bacteria from the genus Anaeroplasma, Ruminococcus, and Butyricicoccus were more enriched in the cancer group. Bacteria from genera Blautia, Akkermansia, Enterococcus, and Coprococcus were more differentially abundant in the Can+Abx group. Bacteria from the genera Lactobacillus, Oscillospira, Ruminococcus, Bifidobacterium, and Anaeroplasma were more enriched in the control group (Figure S3).

Results further highlighted that commensal bacteria were decreased, and pathogenic bacteria were increased with antibiotic treatment. Put together, these results indicate that the gut microbiome may mediate increased pain sensitivity in mice with metastatic breast cancer to bone.

Antibiotic treatment changed the predicted microbiome function in cancer-bearing mice

BugBase algorithm was used to predict high-level phenotypes present in large intestinal microbiome samples using 16S amplicon data. The BugBase phenotype predicted the abundance of gram-positive, gram-negative, biofilm-forming, and potentially pathogenic bacteria. Large intestinal samples from the Can+Abx group had a higher abundance of biofilm-forming ($P < 0.05$) than the cancer group (**Figure 7A**). However, the Cancer group had a higher percentage of pathogenic bacteria ($P < 0.05$) (**Figure 7B**). Additionally, the Can+Abx group had higher percentages of gram-negative bacteria ($P < 0.05$) and lower percentages of gram-positive bacteria ($P < 0.05$) (**Figure 7C**, **7D**). The microbial metagenome was predicted with the PICRUSt algorithm, and functions were categorized with KEGG pathways to elucidate the specific changes in microbial pathways further. In total, 41 KEGG level-2 pathways were predicted among all large intestinal samples (Table S2). Pathways related to cell motility, nucleotide metabolism, translation and replication, and repair were positively correlated with samples from the cancer group (**Figure 7E**). On the other hand, pathways related to energy metabolism, carbohydrate metabolism, signal transduction, metabolism of cofactors and vitamins, and signaling were positively correlated with samples from the Can+Abx group (**Figure 7E**).

Proinflammatory environment following antibiotic-induced microbial dysbiosis promotes cancer cell metastasis to bone and induces increased pain sensitivity

Preexisting Commensal Dysbiosis has been reported as a Host-Intrinsic Regulator of Tissue Inflammation and Tumor Cell Dissemination in Hormone Receptor-Positive Breast Cancer [57]. Chronic inflammation has long been known to be associated with cancer development [58]. An inflammatory condition in the gut microenvironment allows aerobic conditions, causes epithelial cell debris to feed on, and generates excessive mucus thickness that ultimately may be beneficial for the proliferation of certain pathogenic bacterial species. Excessive growth of pathogenic bacteria is proportional to chronic inflammation in the gut environment that drives tumorigenesis. To identify the inflammatory markers in the gut microenvironment due to the antibiotic-induced gut microbial disruption, we collected the serum from the control, BMBC, and antibiotic-treated BMBC groups. Sera from these groups were analyzed for cytokine and chemokine profiling by Luminex assay. As expected, expression of pro-inflammatory cytokines and chemokines were markedly upregulated after antibiotics treatment in the BMBC mouse model. A list of inflammatory chemokines, e.g., CXCL-13, CCL-5, and CCL-7, are found to be upregulated significantly in BMBC groups, which further indicates the presence of abundant pathogenic bacteria leads to inflammatory conditions when compared to BMBC group alone (**Figure 8A**). Interestingly, overexpression of both MMP-9 and G-CSF in antibiotic-treated BMBC group and BMBC alone consistent with our previous observation in BMBC group and indicates the severity of systemic inflammatory conditions in antibiotic-treated BMBC group (**Figure 8B**). Interleukin-4 has been known as anti-inflammatory cytokines that act on mainly suppressing the pro-inflammatory milieu [59]. Strikingly, we noticed that IL-4 expression with anti-inflammatory proper-

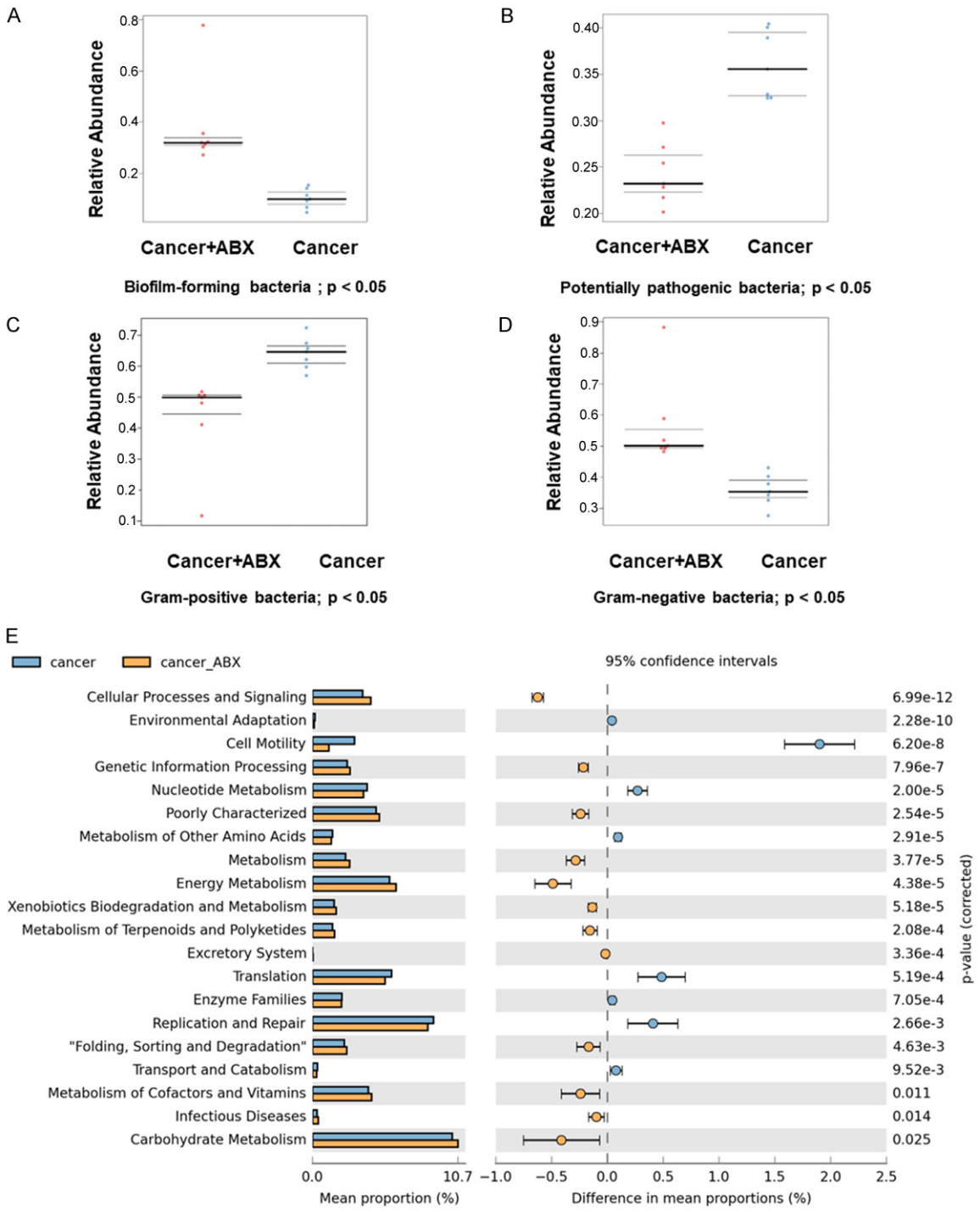

Figure 7. Predictive functional analysis of the gut samples. A. BugBase predicted a relative abundance of biofilm-forming bacteria. P < 0.05 for Cancer vs Cancer+ABX. B. BugBase predicted the relative abundance of potentially pathogenic bacteria. P < 0.05 for Cancer vs Cancer+ABX. C. BugBase predicted the relative abundance of Gram-positive bacteria. P < 0.05 for Cancer vs Cancer+ABX. D. BugBase predicted the relative abundance of Gram-negative bacteria. P < 0.05 for Cancer vs Cancer+ABX. E. The KEGG pathway of gut microbiota was predicted using PICRUSt (Phylogenetic Investigation of Communities by Reconstruction of Unobserved States). Data are presented in a barplot with 95% confidence intervals and *p*-values-samples grouped by Cancer (n=7) and Cancer+Abx (n=7).

ties is downregulated in antibiotic-treated cancer mice compared to sham-treated tumor-bearing mice, which further supports the notion that gut microbial dysbiosis caused by antibiot-

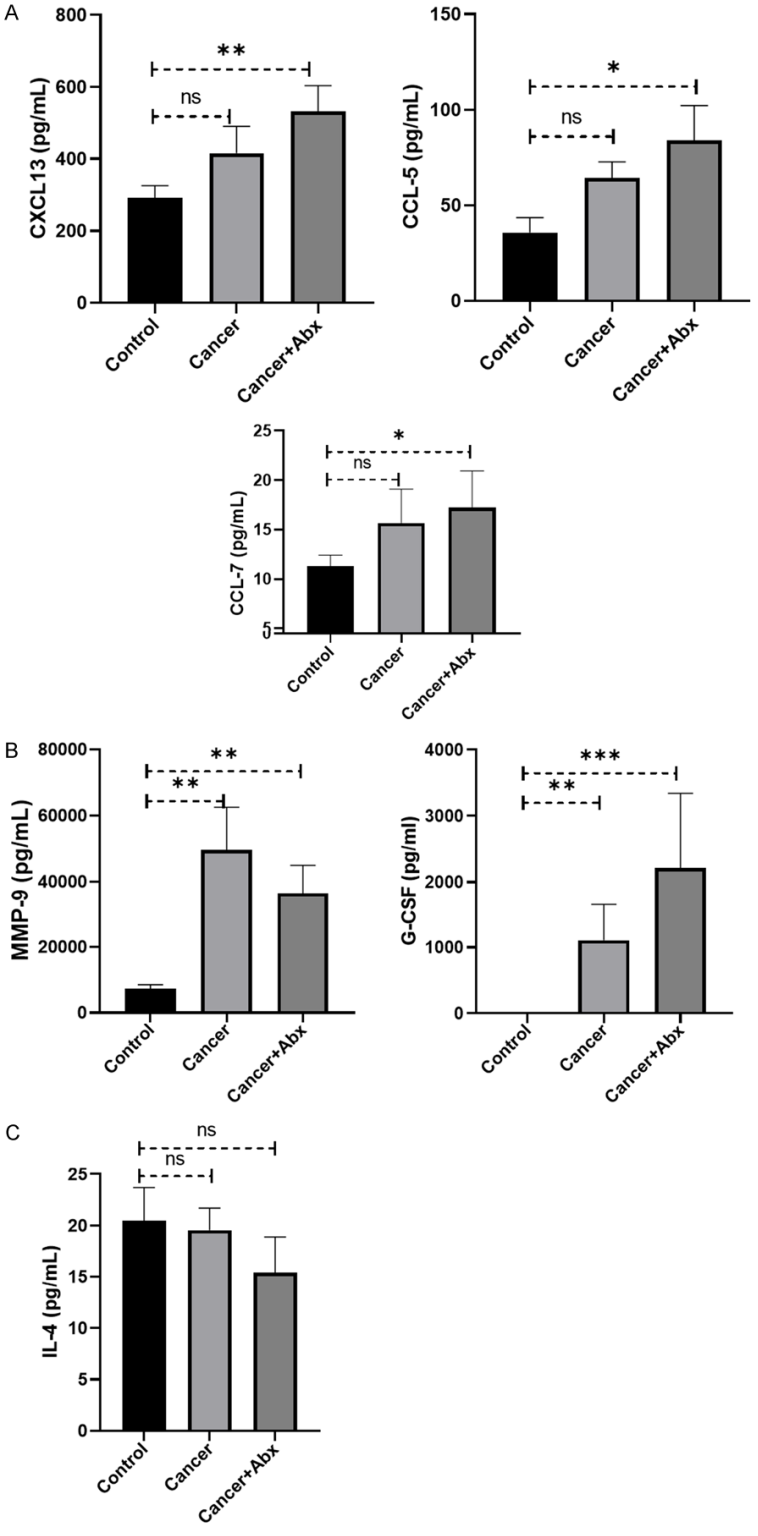

Figure 8. Inflammatory markers (chemokines and cytokines) expression. The serum was collected from control, Bone metastatic breast cancer (BMBC), and Antibiotic treated BMBC mice. CXCL-13, CCL-5, CCL-7, MMP-9, G-CSF, and IL-4 levels were measured and analyzed using Luminex multiplex assay. A. Serum levels of CXCL-13, CCL-5, CCL-7. B. Serum levels of MMP-9 and G-CSF. C. Serum levels of IL-4. n=5-7 group from one experiment was performed, and data was represented as bar plots with SEM. *P < 0.05, **P < 0.005, and ***P < 0.0001 versus naive controls (One-way ANOVA followed by Kruskal-Wallis Test analyzed data).

ic treatment causes excessive but not significant inflammatory milieu in this model (**Figure 8C**).

After that, bone marrow was collected to examine the effect of increased systemic circulation of inflammatory markers on bone metastasis. The composition of immune cells was analyzed using flow cytometry. Flow cytometry results clearly recapitulate our previous observation on immune cell distribution in the BMBC model after cancer cell implantation. Interestingly, the neutrophil population has been increased enough to attract tumor cells to establish an immunosuppressive metastatic niche in the bone microenvironment of the antibiotic-induced BMBC model (**Figure 9A**). As a part of immunosuppressive milieu development, the presence of crucial members of the adaptive immune system (macrophages and B cells) also decreased in both BMBC and antibiotic-treated BMBC animals (**Figure 9B**). In addition, the number of cytotoxic and helper T-cells was reduced in the BM of BMBC mice and antibiotic-treated BMBC mice (**Figure 9C**). These findings suggest that the formation of bone metastases may be associated with immune suppression in the BM. Interestingly, the immune microenvironment in mice inoculated with 4T1-Luc cells was more similar to that of mice inoculated with 4T1-Luc cells and antibiotic treatment. This suggests that a modified immune microenvironment is required for successful metastatic bone colonization.

Inflammation increases in CSF1, which plays a vital role in

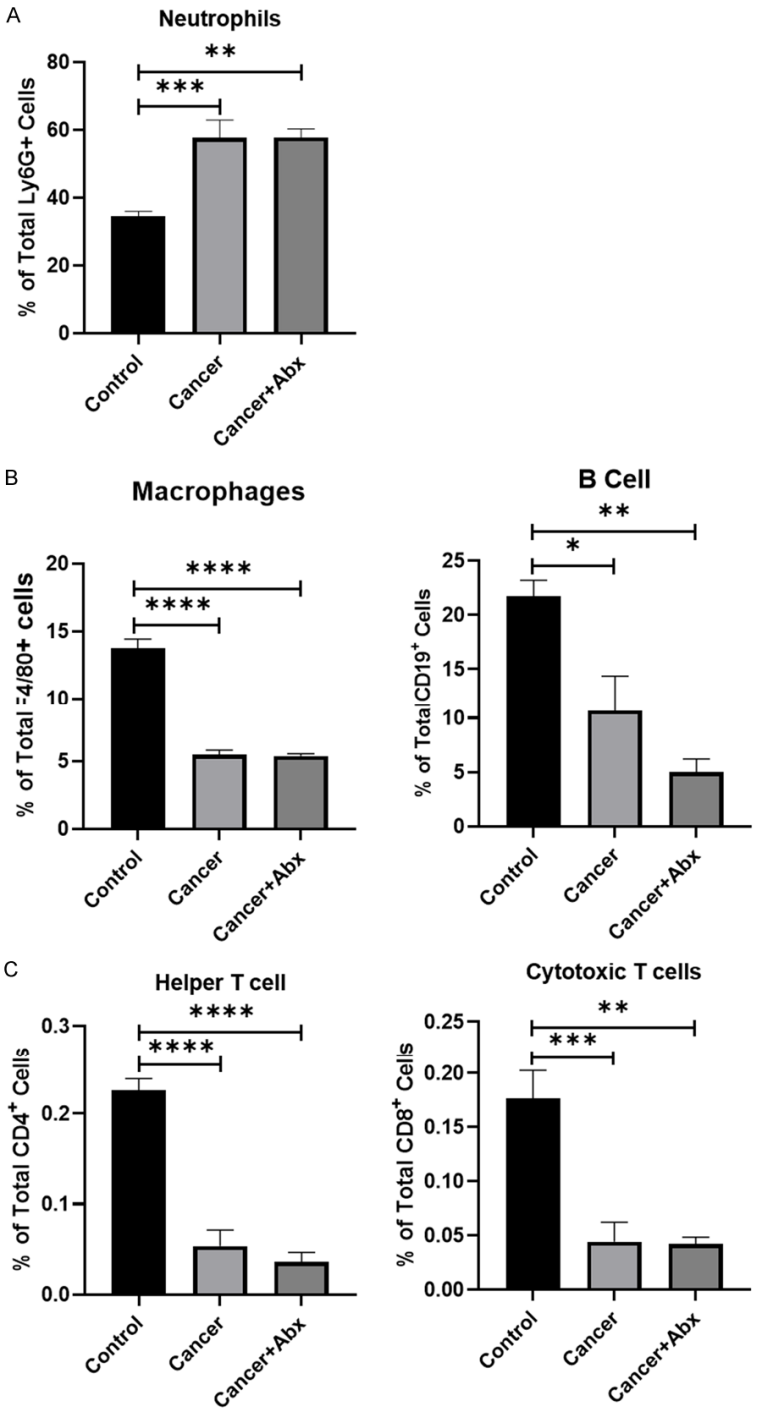

Figure 9. Immunosuppressive environment of bone marrow in bone metastatic breast cancer (BMBC) mouse model followed by antibiotic treatment. (A-C) Bar plots showing mean (SEM) percentages of total Neutrophils (A), Macrophages and B-cells (B), TH-cells and TC-cells (C) as determined by flow cytometry. Data represented as bar plots with SEM. Data were analyzed using one-way ANOVA followed by the Kruskal-Wallis Test. *P < 0.05, **P < 0.01, ***P < 0.001, ****P < 0.0001.

the regulation of osteoclast proliferation and differentiation, and the regulation of bone resorption led us to investigate how inflammation may interact with bone reabsorption. Previous studies have shown that cancer cells can influence osteoclast precursor cells to differentiate and contribute to heightened pain sensitivity [60]. Luminex assay shows an increased expression of inflammatory cytokine G-CSF in antibiotics-treated BMBC mice compared to the control and cancer mice (**Figure 8C**). Increased circulatory G-CSF is associated with neutrophil recruitment to the inflamed tissue and to the bone marrow. Consistent with the Luminex assay, flow cytometric data of bone marrow cells from antibiotics-treated BMBC mice show significant recruitment of neutrophil (Ly6G+) cells compared to control vs cancer mice (**Figure 9A**). Collectively, our results show that inflammation mediated by the gut microbiome may heighten pain sensitivity by recruiting neutrophils that facilitate osteoclasts-mediated breakdown of bone.

Role of gut dysbiosis in nerve/cancer interactions and subsequent pain response

Next, we investigated the role of gut dysbiosis in chemokine and cytokine expression in an in-vitro model (breast cancer cell line (4T1-Luc cells). Earlier, we showed that the antibiotic cocktail induced gut dysbiosis and increased the number of gram-negative bacteria. To interrogate the chemokine and cytokine secretion from breast cancer cell lines in the presence of gram-negative bacteria, we used lipopolysaccharide (LPS) as a surrogate for gram-negative bacteria present in

Table 1. LPS increases inflammatory cytokines and chemokines and promotes pain-associated neuronal markers in Neuro-2a cells

Inflammatory Cytokines and chemokines		Fold Changes
Ccl2		10.12
Ccl20		14.57
Ccl3		3.27
Ccl5		2.22
Ccl7		8.27
Csf1		2.25
Csf3		9.16
Cxcl1		42.48
Cxcl3		15.69
Cxcl5		76.75
Il1a		9.72
Il1b		2.31
Il6		5.46
Tnf		3.69
ptgs		2.2
Ptger4		1.66
Ptges		1.35
Molecular Pathway/ Modulators	Inflammatory Cytokines and chemokines	Fold Change
Neurogenesis	Cxcl1	1.63
	Bmp8b	1.42
Neuroinflammation	Oprk1	1.39
	Trpa1	1.6
Ion Channels	Hcn1	1.65
	Kcna5	2.15
	Kcnj13	1.53
	Kcnj16	2.01
	Kcnj2	1.62
	Trpv3	1.36
	Trpv4	1.56
Neurotransmitters	Chrne	1.75
	Gabrg3	1.61
	Htr1a	1.42
	Htr1f	4.29
	Htr2b	1.62
	Sstr4	1.62
	Tacr1	1.54

Gene expression was evaluated using the RT2 Profiler PCR Array (Biosciences, Qiagen), which represented gene expression in 4T1-Luc and Neuro-2a cells. The list of expression levels of genes is presented as fold-regulation values (those greater than 1.3) compared to those for controls (no treatments). Data is represented from 3 independent experiments and $P < 0.05$.

the gut. We treated 4T1-Luc cells with LPS for 24 hours and determined the expression of chemokines' and cytokines' mRNA using the RT2 profiler PCR kit. These studies showed about 14 chemokines and cytokines were significantly upregulated by LPS in 4T1-Luc cells (**Table 1**). Next, we investigated whether increased cytokine and chemokine secretions affect neuronal cell lines. Therefore, we treated the Neuro-2a cell line with cell culture supernatants of 4T1-Luc cells (after removing LPS by affinity absorption by Polymyxin B) for 24 hours. Using neuronal RT^2 profiler PCR kits, we identified several neuronal makers associated with neuroinflammation and a few neuronal ion channels. Among them, TRPV4, TRPA1, OPRK1, HCN, and KCN have been identified and reported to be involved in metastatic breast cancer-associated pain (**Table 1**) [61-65].

Discussion

Surgery has been offered and considered an advanced option to treat breast cancer patients for centuries [66]. However, surgical procedures have a potential risk of microbial infection. Infection rates for surgical treatment of breast cancer people are higher (3% and 15%) than average for a clean surgical procedure [67]. Most often, prophylactic (pre- or perioperative) antibiotics are prescribed for patients undergoing surgery for breast cancer.

Moreover, recent studies have reported that antibiotic use may not bring the best outcomes for patients who undergo surgery and mastectomy [68]. Recent studies in mice and humans have discovered gut microbial dysbiosis with prophylactic antibiotics may result in more aggressive breast cancer [22, 69]. The most prominent clinical symptom of aggressive tumor growth is associated with bone pain, which is generally localized and metastasizes slowly [70]. Breast cancer then spreads to the bones, leading to bone destruction and severe pain [71]. Bone metastasis is widespread in patients with metastatic breast cancer, and clinical management of bone meta-

static pain is important and challenging. To establish a clinically relevant model, spontaneous breast cancer metastasis to bone was found with a triple-negative cell line (designated 4T1-Luc cells), and bone-seeking cancer cells were characterized in the bone immune microenvironment. Then, we set out to elucidate the mechanism of tumor progression to the bone in the context of using antibiotics and subsequent gut dysbiosis and cancer-induced pain.

The gut microbiota encompasses a repertoire of trillions of microbes residing in the human intestine, which ultimately produces a plethora of metabolites that regulate an array of physiological functions as well as the maintenance of gut health. Recent studies hinted toward a co-evolved communication between gut microbiomes and the human immune system [72]. We have previously shown from our lab that morphine treatment leads to gut microbial dysbiosis, which causes systemic and local intestinal tissue inflammation [73]. A growing body of evidence demonstrated that antibiotic-induced gut dysbiosis causes tumor burden on the metastasis model of breast cancer [23, 74]. Inflammatory signaling pathways were amplified with the resultant alterations in the gut microbiota that have been associated with tumor progression [75]. We evaluated the impact of gut microbiome dysbiosis on tumor growth and associated pain in the BMBC mouse model.

Our study demonstrated that commensal dysbiosis after cancer cell implantation leads to increased tumor cell dissemination and metastatic seeding to the bone and causes severe pain in the BMBC mouse model. 16S rRNA analysis on intestinal samples showed an increased richness in bacterial alpha diversity after cancer cells implant as well as antibiotic treatment group compared to control groups. Additionally, our data also showed a distinct clustering of microbial communities after antibiotic treatment compared to control animals, which agrees with previous findings. At the phylum level, a significant decrease in Firmicutes/Bacteroidetes ratio was observed in the cancer and antibiotic-treated cancer groups compared to the control group. No significant change was observed between the control and antibiotics alone group. Firmicutes/Bacteroidetes ratio has been found as a risk factor for breast cancer progression [76].

Further analysis of the Firmicutes phylum revealed an overgrowth of the pathogenic genus Staphylococcus and a significant depletion of the commensal genus Lactobacillus in the intestinal lumen of antibiotic-treated mice, which further supports our previous finding in the cancer group. Gram-negative bacteria, e.g., Bacteroides, a well-studied pathogenic bacterial genus that is a known contributor toward intestinal inflammation, compromising the epithelial barrier by damaging tight junction function. In contrast, bacterial species belonging to the Lactobacillus genus strengthen the intestinal barrier and tighten junction integrity.

Primary tumors are identified to establish favorable locations for metastasis to distant organs, called the pre-metastatic niche (PMN) [77]. Increasing evidence has been reported that neutrophils play a crucial role in establishing PMNs and an immunosuppressive microenvironment that aids the survival and metastasis of tumor cells [78]. The presence of these neutrophils creates a route for recruiting tumor cells from the bloodstream and tissues into the PMN [79]. The increased populations of neutrophils and macrophages in bone marrow suppress the cytotoxic activity of innate and adaptive killer cells and interact with tumor cells to promote their growth and metastasis [80]. Previous studies from our lab have demonstrated that the expansion of pathogenic bacterial communities leads to neutrophil infiltration in the intestinal tissue. We speculate that infiltrated neutrophils reach the bone microenvironment through systemic circulation and create a metastatic niche by attracting cancer cells to the bone. It has become evident that the interactions of tumor cells with the bone microenvironment play a crucial role in enabling bone metastasis. Cancer cells re-program the surrounding neutrophils in this cancer microenvironment by secreting various cytokines, chemokines, and other factors that facilitate cancer growth and metastatic progression. One earlier study reported that with the presence of granulocyte-colony stimulating factor (G-CSF), postmitotic neutrophils transform into macrophages [81]. Another study conducted by Veglia et al. demonstrated that GM-CSF regulates FATP2 overexpression in neutrophils by activat-

ing the STAT5 transcription factor, allowing immunosuppressive activity and accelerating cancer progression [82]. In our data, we observed a specific response of tissue-infiltrated neutrophils contributing to the depletion of the commensal genus *Lactobacillus* and, simultaneously, leading to the expansion of pathogenic gram-negative bacteria. Therefore, the role of tissue-infiltrated neutrophils in causing gut microbial shift might change immune conditions in the gut microenvironment and further facilitate the migration of tumor cells to a distant location.

We sought to characterize the changes in the immune landscape during bone metastasis formation. We found that bone metastases are associated with an increase in myeloid cells and granulocytes and a decrease in T cells, B cells, and NK cells, suggesting that bone metastasis is characterized by immune suppression. Interestingly, we found that these changes preceded the formation of bone metastases and were evident at early/pre-metastatic stages determined by behavioral experiments and systemically in the blood. Our observation is in agreement with previous findings where transcriptome profiling of patient-matched pairs of primary breast cancer and bone metastases indicated that bone metastatic tumors had reduced numbers of CD8+ T cells, regulatory T cells, and dendritic cells, and elevated levels of M2-like macrophages [83]. Our findings demonstrated that systemic changes due to intestinal microbial dysbiosis and subsequent immune modulation in the bone pre-metastatic niche and acquisition of bone-metastatic capacity are associated with significant immunosuppressive conditions in the bone.

Inflammation is an essential component of the tumor microenvironment, and persistent production of cytokines and chemokines stimulate immune cells to secrete more cytokines that work in both autocrine and paracrine manners, leading to a chronic inflammation state that promotes metastasis in breast cancer patients [10, 84-88]. Recent studies have shown that peripheral nerves (sympathetic, parasympathetic, and sensory) interact with tumor and stromal cells to initiate and progress various solid and hematological malignancies. Furthermore, cancers may reactivate nerve-dependent developmental and regenerative processes to promote their growth and survival (neurogenesis). Cancer cells secrete neurotrophic factors that promote nerve innervation in the tumor microenvironment. Conversely, cancer cells' secretion of neurotrophic growth factors drives the outgrowth of nerves into solid tumors. This reciprocal interaction between neuronal and cancer cells provides new insights into the cellular and molecular bases of cancer-associated severe pain.

Recent studies have shown that the gut microbiota plays a crucial and dynamic role in immune response and neuronal function. In addition, gut microbiota-derived mediators can directly or indirectly affect the tumor microenvironment by regulating the neuronal and tumor cells that modulate the excitability of primary nociceptive neurons and sensitize pain in breast cancer patients. This study found that LPS induced excessive secretion of inflammatory cytokines and chemokines in 4T1-Luc cells. In turn, these inflammatory molecules modulate the secretion of neuro-inflammatory markers, neurotransmitters, and neuronal markers expressed in Neuro-2a cells, which all are part of neurogenesis and well-established regulators involved in neuropathic pain and inflammation in breast cancer patients.

In conclusion, our work has shown that disruption of the gut microbiota during cancer growth and antibiotics treatment has a detrimental impact on breast cancer progression. We identified that antibiotic treatment leads to the loss of a commensal microbiota species and concurrent increased pathogenic bacteria that outcompete beneficial bacteria (commensals) and a reduction in alpha diversity in the intestinal environment. The altered intestinal microbial dysbiosis has the potential to release the "brakes" on tumor growth by re-programming the immune microenvironment in the bone, thus providing a metastatic niche. Favorable niche, combined with immunosuppression, drives bone metastasis and cancer-associated pain. Clinically, when tumor cells disseminate to the bone, quality of life dramatically diminishes and is associated with a lower survival rate. Unfortunately, treatments for bone metastasis at this point are generally palliative. Therefore, there is an urgent need for further research to explore the mechanisms through

which bone metastasis and cancer-associated pain in order to improve the quality of life for breast cancer patients. Recent studies have demonstrated that the gut microbiota have emerged as a likely contributor to bone metastasis. In future studies, we will test the hypothesis that probiotic treatment in a murine model of metastatic breast cancer will attenuate pain associated with metastatic cancer.

Acknowledgements

We thank the DRI Flow Cytometry Core Center for performing Flow Cytometry, the Cancer Model Shared Resource for mouse imaging, and the histology research laboratory directed by the Department of Pathology & Laboratory Medicine for processing and sectioning intestinal samples. This work was supported by the Florida Bank Head Coley FDOH 20B12, National Institute on Drug Abuse (R01DA050542); National Institute on Drug Abuse (R01DA047089); National Institute on Drug Abuse (R01DA044582); National Institute on Drug Abuse (R01DA043252); National Institute on Drug Abuse (R01DA037843); and National Institute on Drug Abuse (R01DA034582).

Disclosure of conflict of interest

None.

Abbreviations

BC, Breast Cancer; IBD, Inflammatory Bowel Disease; BMBC, Bone Metastatic Breast Cancer; OUT, Operational Taxonomic Unit; LDA, Linear Discriminant Analysis; Can+Abx, Cancer+Antibiotics; G-CSF, Granulocyte-Colony-Stimulating Factor; MMP-9, Matrix metalloproteinase-9; PMN, Pre-Metastatic Niche; LPS, Lipopolysaccharide; IEC, Intestinal Epithelial Cells; BM, Bone Marrow.

Address correspondence to: Dr. Sabita Roy, Department of Surgery, Miller School of Medicine, University of Miami, Biomedical Research Building, 1501 NW 10th Ave, Miami, FL 33136, USA. Tel: 305-243-8452; E-mail: sabita.roy@miami.edu

References

[1] Giaquinto AN, Sung H, Miller KD, Kramer JL, Newman LA, Minihan A, Jemal A and Siegel RL. Breast cancer statistics, 2022. CA Cancer J Clin 2022; 72: 524-541.

[2] Shao H and Varamini P. Breast cancer bone metastasis: a narrative review of emerging targeted drug delivery systems. Cells 2022; 11: 388.

[3] Ardakani AHG, Faimali M, Nystrom L, Mesko N, Mughal M, Ware H and Gikas P. Metastatic bone disease: early referral for multidisciplinary care. Cleve Clin J Med 2022; 89: 393-399.

[4] Wu HJ and Wu E. The role of gut microbiota in immune homeostasis and autoimmunity. Gut Microbes 2012; 3: 4-14.

[5] Patangia DV, Anthony Ryan C, Dempsey E, Paul Ross R and Stanton C. Impact of antibiotics on the human microbiome and consequences for host health. Microbiologyopen 2022; 11: e1260.

[6] Wei L, Wen XS and Xian CJ. Chemotherapy-induced intestinal microbiota dysbiosis impairs mucosal homeostasis by modulating toll-like receptor signaling pathways. Int J Mol Sci 2021; 22: 9474.

[7] McKee AM, Kirkup BM, Madgwick M, Fowler WJ, Price CA, Dreger SA, Ansorge R, Makin KA, Caim S, Le Gall G, Paveley J, Leclaire C, Dalby M, Alcon-Giner C, Andrusaite A, Feng TY, Di Modica M, Triulzi T, Tagliabue E, Milling SWF, Weilbaecher KN, Rutkowski MR, Korcsmáros T, Hall LJ and Robinson SD. Antibiotic-induced disturbances of the gut microbiota result in accelerated breast tumor growth. iScience 2021; 24: 103012.

[8] Parhi L, Alon-Maimon T, Sol A, Nejman D, Shhadeh A, Fainsod-Levi T, Yajuk O, Isaacson B, Abed J, Maalouf N, Nissan A, Sandbank J, Yehuda-Shnaidman E, Ponath F, Vogel J, Mandelboim O, Granot Z, Straussman R and Bachrach G. Breast cancer colonization by Fusobacterium nucleatum accelerates tumor growth and metastatic progression. Nat Commun 2020; 11: 3259.

[9] Lobionda S, Sittipo P, Kwon HY and Lee YK. The role of gut microbiota in intestinal inflammation with respect to diet and extrinsic stressors. Microorganisms 2019; 7: 271.

[10] Kartikasari AER, Huertas CS, Mitchell A and Plebanski M. Tumor-induced inflammatory cytokines and the emerging diagnostic devices for cancer detection and prognosis. Front Oncol 2021; 11: 692142.

[11] Pal S, Perrien DS, Yumoto T, Faccio R, Stoica A, Adams J, Coopersmith CM, Jones RM, Weitzmann MN and Pacifici R. The microbiome restrains melanoma bone growth by promoting intestinal NK and Th1 cell homing to bone. J Clin Invest 2022; 132: e157340.

[12] Wu M, Ma M, Tan Z, Zheng H and Liu X. Neutrophil: a new player in metastatic cancers. Front Immunol 2020; 11: 565165.

[13] Thio QCBS, Goudriaan WA, Janssen SJ, Paulino Pereira NR, Sciubba DM, Rosovksy RP and Schwab JH. Prognostic role of neutrophil-to-lymphocyte ratio and platelet-to-lymphocyte ratio in patients with bone metastases. Br J Cancer 2018; 119: 737-743.
[14] Giese MA, Hind LE and Huttenlocher A. Neutrophil plasticity in the tumor microenvironment. Blood 2019; 133: 2159-2167.
[15] Spiegel A, Brooks MW, Houshyar S, Reinhardt F, Ardolino M, Fessler E, Chen MB, Krall JA, DeCock J, Zervantonakis IK, Iannello A, Iwamoto Y, Cortez-Retamozo V, Kamm RD, Pittet MJ, Raulet DH and Weinberg RA. Neutrophils suppress intraluminal NK cell-mediated tumor cell clearance and enhance extravasation of disseminated carcinoma cells. Cancer Discov 2016; 6: 630-649.
[16] Casbon AJ, Reynaud D, Park C, Khuc E, Gan DD, Schepers K, Passegué E and Werb Z. Invasive breast cancer reprograms early myeloid differentiation in the bone marrow to generate immunosuppressive neutrophils. Proc Natl Acad Sci U S A 2015; 112: E566-E575.
[17] Weigelt B, Peterse JL and van't Veer LJ. Breast cancer metastasis: markers and models. Nat Rev Cancer 2005; 5: 591-602.
[18] Le Pape F, Vargas G and Clézardin P. The role of osteoclasts in breast cancer bone metastasis. J Bone Oncol 2016; 5: 93-95.
[19] Chen YC, Sosnoski DM and Mastro AM. Breast cancer metastasis to the bone: mechanisms of bone loss. Breast Cancer Res 2010; 12: 215.
[20] Restaino AC and Vermeer PD. Neural regulations of the tumor microenvironment. FASEB Bioadv 2021; 4: 29-42.
[21] Mizumura K and Murase S. Role of nerve growth factor in pain. Handb Exp Pharmacol 2015; 227: 57-77.
[22] Ransohoff JD, Ritter V, Purington N, Andrade K, Han S, Liu M, Liang SY, John EM, Gomez SL, Telli ML, Schapira L, Itakura H, Sledge GW, Bhatt AS and Kurian AW. Antimicrobial exposure is associated with decreased survival in triple-negative breast cancer. Nat Commun 2023; 14: 2053.
[23] Buchta Rosean C, Bostic RR, Ferey JCM, Feng TY, Azar FN, Tung KS, Dozmorov MG, Smirnova E, Bos PD and Rutkowski MR. Preexisting commensal dysbiosis is a host-intrinsic regulator of tissue inflammation and tumor cell dissemination in hormone receptor-positive breast cancer. Cancer Res 2019; 79: 3662-3675.
[24] Chen YC, Sosnoski DM and Mastro AM. Breast cancer metastasis to the bone: mechanisms of bone loss. Breast Cancer Res 2010; 12: 215.
[25] Russo S, Scotto di Carlo F and Gianfrancesco F. The osteoclast traces the route to bone tumors and metastases. Front Cell Dev Biol 2022; 10: 886305.
[26] Vičić I and Belev B. The pathogenesis of bone metastasis in solid tumors: a review. Croat Med J 2021; 62: 270-282.
[27] Callahan BJ, McMurdie PJ, Rosen MJ, Han AW, Johnson AJ and Holmes SP. DADA2: high-resolution sample inference from Illumina amplicon data. Nat Methods 2016; 13: 581-3.
[28] Bolyen E, Rideout JR, Dillon MR, Bokulich NA, Abnet CC, Al-Ghalith GA, Alexander H, Alm EJ, Arumugam M, Asnicar F, Bai Y, Bisanz JE, Bittinger K, Brejnrod A, Brislawn CJ, Brown CT, Callahan BJ, Caraballo-Rodríguez AM, Chase J, Cope EK, Da Silva R, Diener C, Dorrestein PC, Douglas GM, Durall DM, Duvallet C, Edwardson CF, Ernst M, Estaki M, Fouquier J, Gauglitz JM, Gibbons SM, Gibson DL, Gonzalez A, Gorlick K, Guo J, Hillmann B, Holmes S, Holste H, Huttenhower C, Huttley GA, Janssen S, Jarmusch AK, Jiang L, Kaehler BD, Kang KB, Keefe CR, Keim P, Kelley ST, Knights D, Koester I, Kosciolek T, Kreps J, Langille MGI, Lee J, Ley R, Liu YX, Loftfield E, Lozupone C, Maher M, Marotz C, Martin BD, McDonald D, McIver LJ, Melnik AV, Metcalf JL, Morgan SC, Morton JT, Naimey AT, Navas-Molina JA, Nothias LF, Orchanian SB, Pearson T, Peoples SL, Petras D, Preuss ML, Pruesse E, Rasmussen LB, Rivers A, Robeson MS 2nd, Rosenthal P, Segata N, Shaffer M, Shiffer A, Sinha R, Song SJ, Spear JR, Swafford AD, Thompson LR, Torres PJ, Trinh P, Tripathi A, Turnbaugh PJ, Ul-Hasan S, van der Hooft JJJ, Vargas F, Vázquez-Baeza Y, Vogtmann E, von Hippel M, Walters W, Wan Y, Wang M, Warren J, Weber KC, Williamson CHD, Willis AD, Xu ZZ, Zaneveld JR, Zhang YL, Zhu QY, Knight R and Gregory Caporaso J. Reproducible, interactive, scalable and extensible microbiome data science using QIIME 2. Nat Biotechnol 2019; 37: 852-857.
[29] Bokulich NA, Kaehler BD, Rideout JR, Dillon M, Bolyen E, Knight R, Huttley GA and Gregory Caporaso J. Optimizing taxonomic classification of marker-gene amplicon sequences with QIIME 2's q2-feature-classifier plugin. Microbiome 2018; 6: 90.
[30] McDonald D, Price MN, Goodrich J, Nawrocki EP, DeSantis TZ, Probst A, Andersen GL, Knight R and Hugenholtz P. An improved Greengenes taxonomy with explicit ranks for ecological and evolutionary analyses of bacteria and archaea. ISME J 2012; 6: 610-618.
[31] Chong J, Liu P, Zhou G and Xia J. Using MicrobiomeAnalyst for comprehensive statistical, functional, and meta-analysis of microbiome data. Nat Protoc 2020; 15: 799-821.
[32] Segata N, Izard J, Waldron L, Gevers D, Miropolsky L, Garrett WS and Huttenhower C. Metage-

nomic biomarker discovery and explanation. Genome Biol 2011; 12: R60.
[33] Langille MG, Zaneveld J, Caporaso JG, McDonald D, Knights D, Reyes JA, Clemente JC, Burkepile DE, Vega Thurber RL, Knight R, Beiko RG and Huttenhower C. Predictive functional profiling of microbial communities using 16S rRNA marker gene sequences. Nat Biotechnol 2013; 31: 814-821.
[34] Markowitz VM, Chen IM, Palaniappan K, Chu K, Szeto E, Grechkin Y, Ratner A, Jacob B, Huang J, Williams P, Huntemann M, Anderson I, Mavromatis K, Ivanova NN and Kyrpides NC. IMG: the integrated microbial genomes database and comparative analysis system. Nucleic Acids Res 2012; 40: D115-D122.
[35] Kanehisa M, Sato Y, Kawashima M, Furumichi M and Tanabe M. KEGG as a reference resource for gene and protein annotation. Nucleic Acids Res 2016; 44: D457-D462.
[36] Parks DH, Tyson GW, Hugenholtz P and Beiko RG. STAMP: statistical analysis of taxonomic and functional profiles. Bioinformatics 2014; 30: 3123-3124.
[37] Ward T, Larson J, Meulemans J, Hillmann B, Lynch J, Sidiropoulos D, Spear JR, Caporaso G, Blekhman R and Knight R. BugBase predicts organism-level microbiome phenotypes. BioRxiv 2017; 133462.
[38] Paschall AV and Liu K. An orthotopic mouse model of spontaneous breast cancer metastasis. J Vis Exp 2016; 54040.
[39] Pulaski BA and Ostrand-Rosenberg S. Mouse 4T1 breast tumor model. Curr Protoc Immunol 2001; Chapter 20: Unit 20.2.
[40] Rashid NS, Grible JM, Clevenger CV and Harrell JC. Breast cancer liver metastasis: current and future treatment approaches. Clin Exp Metastasis 2021; 38: 263-277.
[41] Xu Z, Yuan JJ, Jiang J and Ma L. Liver metastasis occurring within four months of early breast cancer diagnosis: a case report and literature review. Case Rep Oncol 2022; 15: 827-832.
[42] Lin B, Wang Y, Zhang P, Yuan Y, Zhang Y and Chen G. Gut microbiota regulates neuropathic pain: potential mechanisms and therapeutic strategy. J Headache Pain 2020; 21: 103.
[43] Guo R, Chen LH, Xing C and Liu T. Pain regulation by gut microbiota: molecular mechanisms and therapeutic potential. Br J Anaesth 2019; 123: 637-654.
[44] Panis C and Pavanelli WR. Cytokines as mediators of pain-related process in breast cancer. Mediators Inflamm 2015; 2015: 129034.
[45] Panis C, Victorino VJ, Herrera AC, Freitas LF, De Rossi T, Campos FC, Simão AN, Barbosa DS, Pinge-Filho P, Cecchini R and Cecchini AL. Differential oxidative status and immune characterization of the early and advanced stages of human breast cancer. Breast Cancer Res Treat 2012; 133: 881-888.
[46] Mousa WK, Chehadeh F and Husband S. Microbial dysbiosis in the gut drives systemic autoimmune diseases. Front Immunol 2022; 13: 906258.
[47] DeGruttola AK, Low D, Mizoguchi A and Mizoguchi E. Current understanding of dysbiosis in disease in human and animal models. Inflamm Bowel Dis 2016; 22: 1137-1150.
[48] Liu T, Zhang L, Joo D and Sun SC. NF-κB signaling in inflammation. Signal Transduct Target Ther 2017; 2: 17023.
[49] Ławicki S, Będkowska GE, Wojtukiewicz M and Szmitkowski M. Hematopoietic cytokines as tumor markers in breast malignancies. A multivariate analysis with ROC curve in breast cancer patients. Adv Med Sci 2013; 58: 207-215.
[50] Chistiakov DA, Bobryshev YV, Kozarov E, Sobenin IA and Orekhov AN. Intestinal mucosal tolerance and impact of gut microbiota to mucosal tolerance. Front Microbiol 2015; 5: 781.
[51] Desalegn G and Pabst O. Inflammation triggers immediate rather than progressive changes in monocyte differentiation in the small intestine. Nat Commun 2019; 10: 3229.
[52] Pujada A, Walter L, Patel A, Bui TA, Zhang Z, Zhang Y, Denning TL and Garg P. Matrix metalloproteinase MMP9 maintains epithelial barrier function and preserves mucosal lining in colitis associated cancer. Oncotarget 2017; 8: 94650-94665.
[53] Joseph C, Alsaleem M, Orah N, Narasimha PL, Miligy IM, Kurozumi S, Ellis IO, Mongan NP, Green AR and Rakha EA. Elevated MMP9 expression in breast cancer is a predictor of shorter patient survival. Breast Cancer Res Treat 2020; 182: 267-282.
[54] Zhuang J, Zhang J, Lwin ST, Edwards JR, Edwards CM, Mundy GR and Yang X. Osteoclasts in multiple myeloma are derived from Gr-1+CD11b+myeloid-derived suppressor cells. PLoS One 2012; 7: e48871.
[55] Mutlu EA, Keshavarzian A, Losurdo J, Swanson G, Siewe B, Forsyth C, French A, DeMarais P, Sun Y, Koenig L, Cox S, Engen P, Chakradeo P, Abbasi R, Gorenz A, Burns C and Landay A. A compositional look at the human gastrointestinal microbiome and immune activation parameters in HIV infected subjects. PLoS Pathog 2014; 10: e1003829.
[56] Morrell S, Kohonen-Corish MRJ, Ward RL, Sorrell TC, Roder D and Currow DC. Antibiotic exposure within six months before systemic therapy was associated with lower cancer survival. J Clin Epidemiol 2022; 147: 122-131.
[57] Buchta Rosean C, Bostic RR, Ferey JCM, Feng TY, Azar FN, Tung KS, Dozmorov MG, Smirnova E, Bos PD and Rutkowski MR. Preexisting com-

mensal dysbiosis is a host-intrinsic regulator of tissue inflammation and tumor cell dissemination in hormone receptor-positive breast cancer. Cancer Res 2019; 79: 3662-3675.
[58] Singh N, Baby D, Rajguru JP, Patil PB, Thakkannavar SS and Pujari VB. Inflammation and cancer. Ann Afr Med 2019; 18: 121-126.
[59] Chatterjee P, Chiasson VL, Bounds KR and Mitchell BM. Regulation of the anti-inflammatory cytokines interleukin-4 and interleukin-10 during pregnancy. Front Immunol 2014; 5: 253.
[60] Andriessen AS, Donnelly CR and Ji RR. Reciprocal interactions between osteoclasts and nociceptive sensory neurons in bone cancer pain. Pain Rep 2021; 6: e867.
[61] Li XY, He C, Zhu Y and Lu NH. Role of gut microbiota on intestinal barrier function in acute pancreatitis. World J Gastroenterol 2020; 26: 2187-2193.
[62] de Almeida AS, Pereira GC, Brum EDS, Silva CR, Antoniazzi CTD, Ardisson-Araújo D, Oliveira SM and Trevisan G. Role of TRPA1 expressed in bone tissue and the antinociceptive effect of the TRPA1 antagonist repeated administration in a breast cancer pain model. Life Sci 2021; 276: 119469.
[63] Li H, Ma Z and Lei Y. The expression of kappa-opioid receptor promotes the migration of breast cancer cells in vitro. BMC Anesthesiol 2021; 21: 210.
[64] Lei X, Yan Y, Zeng J, Wang R, Li S, Xiao Z and Liu X. Activation of HCN channels caused by elevated cAMP levels in periaqueductal gray promotes bone cancer pain. Neurochem Int 2023; 162: 105437.
[65] Hou X, Tang L, Li X, Xiong F, Mo Y, Jiang X, Deng X, Peng M, Wu P, Zhao M, Ouyang J, Shi L, He Y, Yan Q, Zhang S, Gong Z, Li G, Zeng Z, Wang F, Guo C and Xiong W. Potassium channel protein KCNK6 promotes breast cancer cell proliferation, invasion, and migration. Front Cell Dev Biol 2021; 9: 616784.
[66] Czajka ML and Pfeifer C. Breast cancer surgery. Treasure Island (FL) ineligible companies. StatPearls; 2023.
[67] Prudencio RMA, Campos FSM, Loyola ABAT, Archangelo Junior I, Novo NF, Ferreira LM and Veiga DF. Antibiotic prophylaxis in breast cancer surgery. A randomized controlled trial. Acta Cir Bras 2020; 35: e202000907.
[68] Sisco M, Kuchta K, Alva D and Seth AK. Oral antibiotics do not prevent infection or implant loss after immediate prosthetic breast reconstruction. Plast Reconstr Surg 2023; 151: 730e-738e.
[69] McKee AM, Kirkup BM, Madgwick M, Fowler WJ, Price CA, Dreger SA, Ansorge R, Makin KA, Caim S, Le Gall G, Paveley J, Leclaire C, Dalby M, Alcon-Giner C, Andrusaite A, Feng TY, Di Modica M, Triulzi T, Tagliabue E, Milling SWF, Weilbaecher KN, Rutkowski MR, Korcsmáros T, Hall LJ and Robinson SD. Antibiotic-induced disturbances of the gut microbiota result in accelerated breast tumor growth. iScience 2021; 24: 103012.
[70] Chin H and Kim J. Bone metastasis: concise overview. Fed Pract 2015; 32: 24-30.
[71] Tahara RK, Brewer TM, Theriault RL and Ueno NT. Bone metastasis of breast cancer. Adv Exp Med Biol 2019; 1152: 105-129.
[72] Laborda-Illanes A, Sanchez-Alcoholado L, Dominguez-Recio ME, Jimenez-Rodriguez B, Lavado R, Comino-Méndez I, Alba E and Queipo-Ortuño MI. Breast and gut microbiota action mechanisms in breast cancer pathogenesis and treatment. Cancers (Basel) 2020; 12: 2465.
[73] Wang F, Meng J, Zhang L, Johnson T, Chen C and Roy S. Morphine induces changes in the gut microbiome and metabolome in a morphine dependence model. Sci Rep 2018; 8: 3596.
[74] McKee AM, Kirkup BM, Madgwick M, Fowler WJ, Price CA, Dreger SA, Ansorge R, Makin KA, Caim S, Le Gall G, Paveley J, Leclaire C, Dalby M, Alcon-Giner C, Andrusaite A, Feng TY, Di Modica M, Triulzi T, Tagliabue E, Milling SWF, Weilbaecher KN, Rutkowski MR, Korcsmáros T, Hall LJ and Robinson SD. Antibiotic-induced disturbances of the gut microbiota result in accelerated breast tumor growth. iScience 2021; 24: 103012.
[75] Zitvogel L, Galluzzi L, Viaud S, Vétizou M, Daillère R, Merad M and Kroemer G. Cancer and the gut microbiota: an unexpected link. Sci Transl Med 2015; 7: 271ps1.
[76] An J, Kwon H and Kim YJ. The firmicutes/bacteroidetes ratio as a risk factor of breast cancer. J Clin Med 2023; 12: 2216.
[77] Kaplan RN, Riba RD, Zacharoulis S, Bramley AH, Vincent L, Costa C, MacDonald DD, Jin DK, Shido K, Kerns SA, Zhu Z, Hicklin D, Wu Y, Port JL, Altorki N, Port ER, Ruggero D, Shmelkov SV, Jensen KK, Rafii S and Lyden D. VEGFR1-positive haematopoietic bone marrow progenitors initiate the pre-metastatic niche. Nature 2005; 438: 820-827.
[78] Faget J, Peters S, Quantin X, Meylan E and Bonnefoy N. Neutrophils in the era of immune checkpoint blockade. J Immunother Cancer 2021; 9: e002242.
[79] Wculek SK and Malanchi I. Neutrophils support lung colonization of metastasis-initiating breast cancer cells. Nature 2015; 528: 413-417.
[80] Güç E and Pollard JW. Redefining macrophage and neutrophil biology in the metastatic cascade. Immunity 2021; 54: 885-902.

[81] Araki H, Katayama N, Yamashita Y, Mano H, Fujieda A, Usui E, Mitani H, Ohishi K, Nishii K, Masuya M, Minami N, Nobori T and Shiku H. Reprogramming of human postmitotic neutrophils into macrophages by growth factors. Blood 2004; 103: 2973-2980.

[82] Veglia F, Tyurin VA, Blasi M, De Leo A, Kossenkov AV, Donthireddy L, To TKJ, Schug Z, Basu S, Wang F, Ricciotti E, DiRusso C, Murphy ME, Vonderheide RH, Lieberman PM, Mulligan C, Nam B, Hockstein N, Masters G, Guarino M, Lin C, Nefedova Y, Black P, Kagan VE and Gabrilovich DI. Fatty acid transport protein 2 reprograms neutrophils in cancer. Nature 2019; 569: 73-78.

[83] Zhu L, Narloch JL, Onkar S, Joy M, Broadwater G, Luedke C, Hall A, Kim R, Pogue-Geile K, Sammons S, Nayyar N, Chukwueke U, Brastianos PK, Anders CK, Soloff AC, Vignali DAA, Tseng GC, Emens LA, Lucas PC, Blackwell KL, Oesterreich S and Lee AV. Metastatic breast cancers have reduced immune cell recruitment but harbor increased macrophages relative to their matched primary tumors. J Immunother Cancer 2019; 7: 265.

[84] Mollica Poeta V, Massara M, Capucetti A and Bonecchi R. Chemokines and chemokine receptors: new targets for cancer immunotherapy. Front Immunol 2019; 10: 379.

[85] Li H, Wu M and Zhao X. Role of chemokine systems in cancer and inflammatory diseases. MedComm (2020) 2022; 3: e147.

[86] Singh R, Lillard JW Jr and Singh S. Chemokines: key players in cancer progression and metastasis. Front Biosci (Schol Ed) 2011; 3: 1569-1582.

[87] Sarvaiya PJ, Guo D, Ulasov I, Gabikian P and Lesniak MS. Chemokines in tumor progression and metastasis. Oncotarget 2013; 4: 2171-2185.

[88] Esquivel-Velázquez M, Ostoa-Saloma P, Palacios-Arreola MI, Nava-Castro KE, Castro JI and Morales-Montor J. The role of cytokines in breast cancer development and progression. J Interferon Cytokine Res 2015; 35: 1-16.

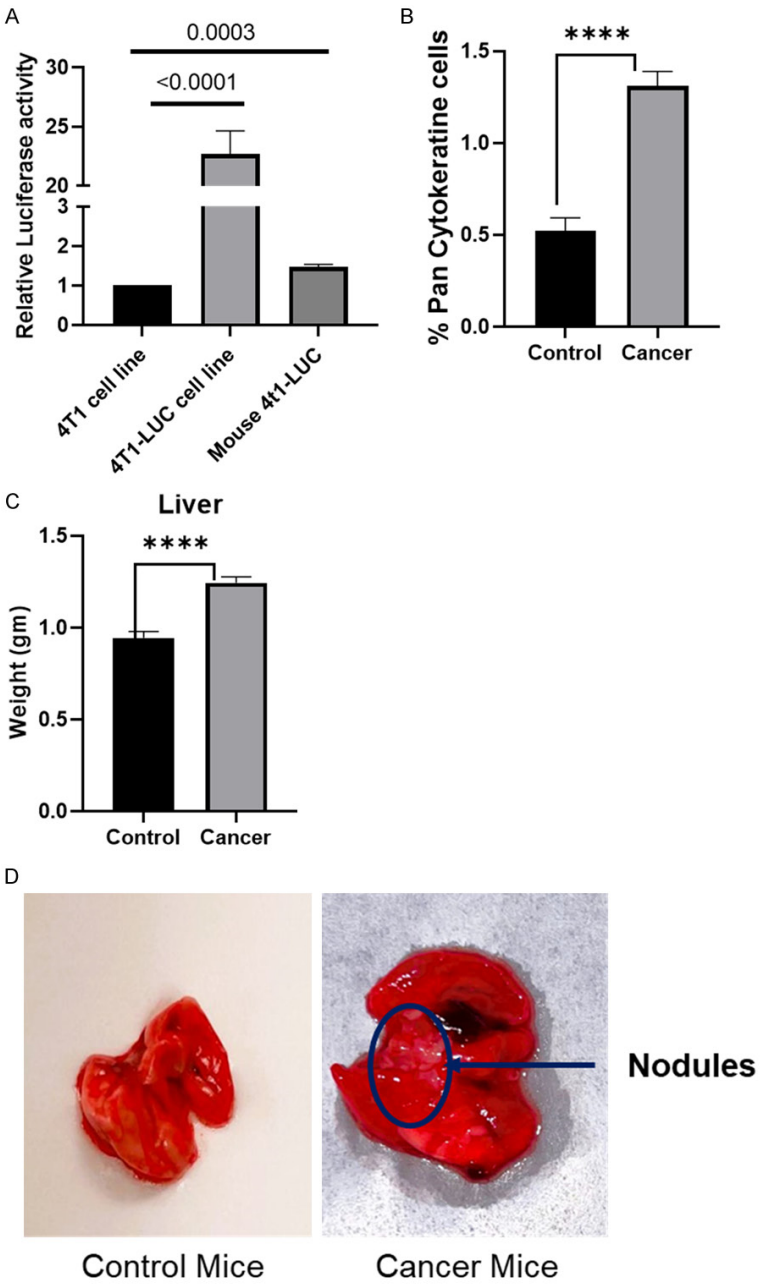

Figure S1. Bone metastatic breast cancer murine model. A. Bone marrow was collected from an orthotopic mouse model 21 days post-injection with the 4T1-Luc cell line. Luciferase activity was measured from the bone marrow cells incubated with luciferin. 4T1 cell lines with or without luciferase were used for comparative analysis. n=4 independent replicates with 4T1 cells and 4T1-Luc cells. n= bone marrow from 4 cancer mice. B. Bone marrow cells were stained with Pan-cytokeratin antibody to detect the epithelial cells in the bone marrow and confirm bone metastasis. n=5 control mice and n=10 cancer mice. C. Liver from the treatment groups were collected at the time of sacking to detect metastasis by weighing the mass. n=10 mice per treatment group. D. Lung metastasis was identified with the presence of the nodules on the surface collected from the metastatic cancer mice. *P* values were calculated using the student's two-tailed t-test. Data are represented as mean ± SEM.

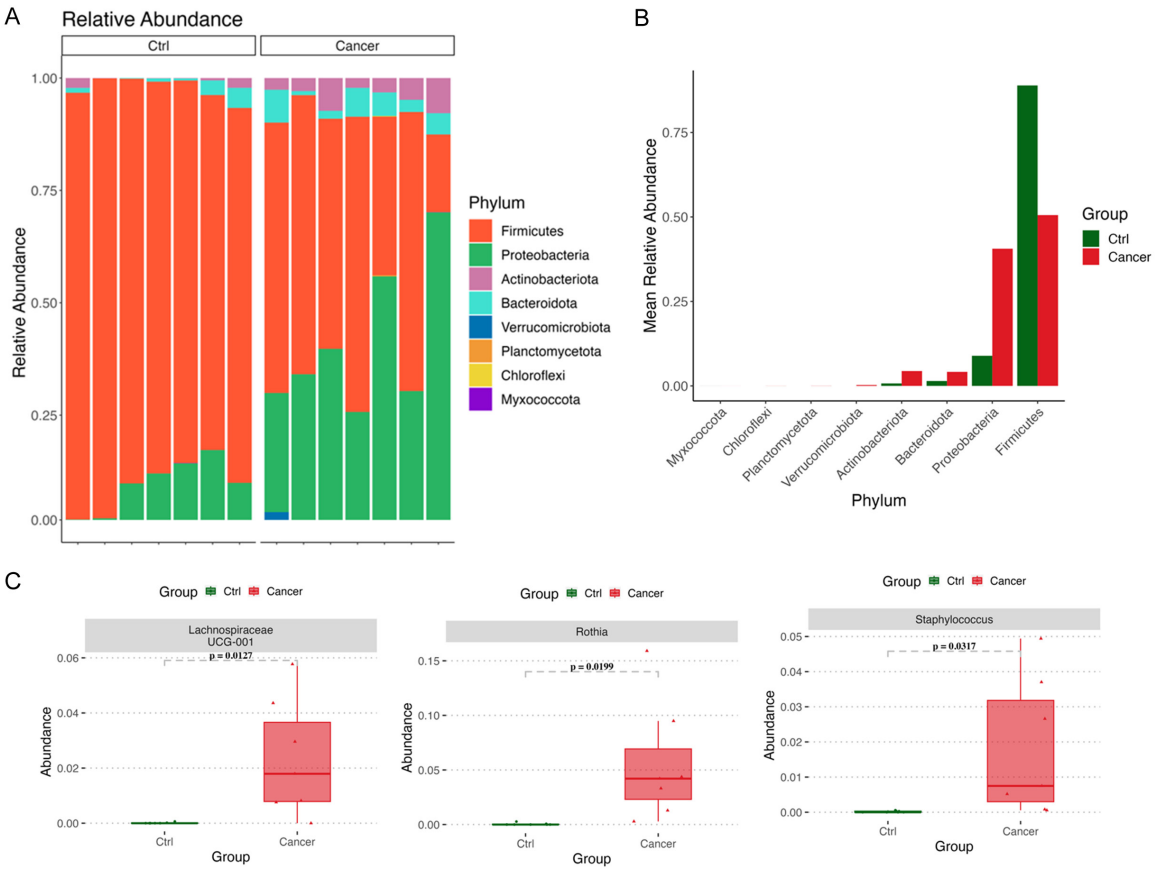

Figure S2. A reduced Firmicutes to Bacteroidetes ratio was observed after cancer cell implantation in cancer mice. A. Taxonomic distribution at the phylum level, showing individual samples. B. Cancer cell implantation of increased pathogenic bacteria at the phylum level signifies an increased level of inflammation. C. Accelerated growth of Staphylococcus, Rothia, and Lachnospiraceae supports the gut microbial dysbiosis after cancer cell implantation and increased pain sensation in the cancer mice group.

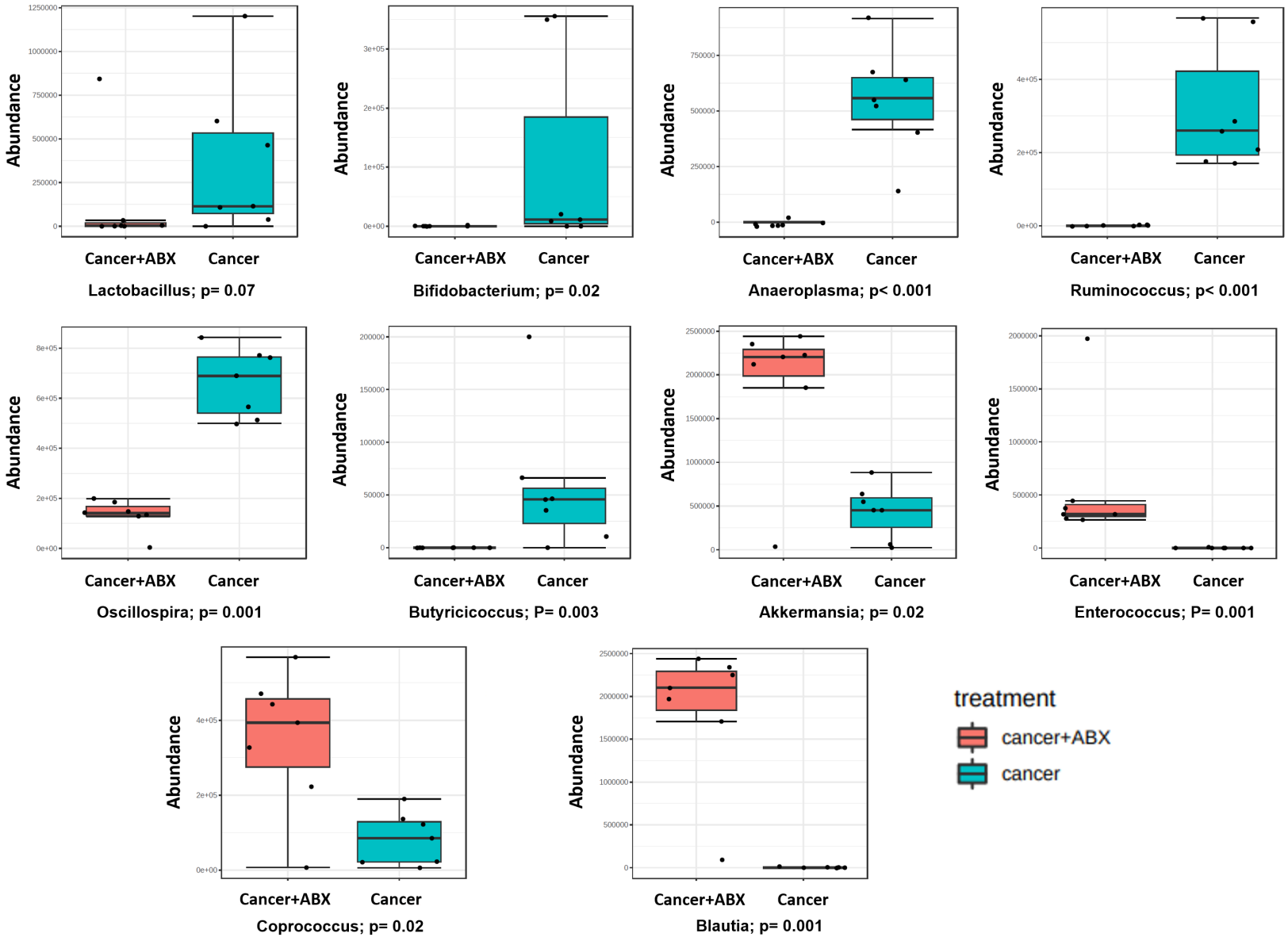

Figure S3. Alteration of gut microbiome at the genus level following antibiotic treatment. Box plots of bacteria genera were differentially enriched between Cancer (n=7) and Can+Abx (n=7). All genera have higher than 2 log LDA scores and lower than 0.1 FDR-adjusted *p*-value.